Geol. Mag. **155** (*2*), *2018, pp. 451–478. © Cambridge University Press 2017*
doi:10.1017/S0016756817000401

The Jurassic–Early Cretaceous basalt–chert association in the ophiolites of the Ankara Mélange, east of Ankara, Turkey: age and geochemistry

VALERIO BORTOLOTTI*, MARCO CHIARI‡†, M. CEMAL GÖNCÜOGLU§, GIANFRANCO PRINCIPI*, EMILIO SACCANI¶, U. KAGAN TEKIN|| & RENZO TASSINARI¶

*Dipartimento di Scienze della Terra, Università degli Studi di Firenze, Via G. La Pira 4, 50121 Firenze, Italy
‡CNR, Istituto di Geoscienze e Georisorse, Via G. La Pira 4, 50121 Firenze, Italy
§Geological Engineering Department, Middle East Technical University, 06531, Ankara, Turkey
¶Dipartimento di Fisica e Scienze della Terra, Università degli Studi di Ferrara, Via Saragat 1, 44122 Ferrara, Italy
||Geological Engineering Department, Hacettepe University, 06532, Beytepe, Ankara, Turkey

(*Received* 30 October 2016; *accepted* 10 April 2017; *first published online* 6 June 2017)

Abstract – This study is focused on slide blocks including oceanic lavas associated with pelagic sediments within the eastern part of the Ankara Mélange. A detailed petrological characterization of the volcanic rocks and a detailed biochronological investigation of the associated radiolarian cherts in eight sections (east of Ankara) was carried out. The volcanic rocks are largely represented by basalts and minor ferrobasalts and trachytes. They show different geochemical affinities and overlapping ages including: (a) Late Jurassic – Early Cretaceous garnet-influenced MORB (middle late Oxfordian to late Kimmeridgian–early Tithonian and early–early late Tithonian; late Valanginian–early Barremian); (b) Early Cretaceous enriched-MORB (middle late Barremian–early early Aptian; Valanginian to middle Aptian–early Albian); (c) Middle Jurassic plume-type MORB (early–middle Bajocian to late Bathonian–early Callovian); (d) Late Jurassic – Early Cretaceous alkaline basalts (middle–late Oxfordian to late Kimmeridgian–early Tithonian; late Valanginian to late Hauterivian). All rock types show a clear garnet signature, as testified to by their high MREE/HREE (middle rare earth element/heavy rare earth element) ratios. The coexistence of chemically different rock types from Middle Jurassic to Early Cretaceous times suggests that they were formed in a mid-ocean ridge setting from partial melting of a highly heterogeneous mantle characterized by the extensive occurrence of OIB-metasomatized portions, which were likely inherited from Triassic mantle plume activity associated with the continental rift and opening of the Neotethys branch.

Keywords: ophiolites, geochemistry, radiolarian biostratigraphy, Jurassic, Early Cretaceous, Ankara Mélange, Turkey

1. Introduction

Despite numerous studies since the 1960s in Turkey, the locations, ages and geological evolution of the branches of the Eastern Mesozoic Tethys Ocean or Eastern Neotethys are disputed (see Sengör & Yılmaz, 1981; Dercourt *et al.* 1986; Robertson *et al.* 1996; Göncüoglu, Dirik & Kozlu, 1997; Dilek *et al.* 1999; Göncüoglu *et al*. 2000; Stampfli & Borel, 2002; Bortolotti & Principi, 2005; Göncüoglu, Yaliniz & Tekin, 2006; Schmid *et al.* 2008; Moix *et al.* 2008; Göncüoglu, Sayit & Tekin, 2010). This is mainly owing to two deficiencies. One of them is the fact that next to definite ophiolitic suture belts separating continental blocks with distinct geological histories there are also suture-like alignments or pseudo-belts of allochthonous ophiolitic bodies. The second shortcoming regards the method of ophiolite research yet realized, as it was rarely based upon a multidisciplinary approach. Several detailed petrological studies on different units from different ophiolitic bodies lack age data and vice versa. A considerable number of studies were concentrated on the larger and more or less complete ophiolitic bodies and neglected the remarkable amount of basalt–radiolarian chert associations within the mélange complexes. To overcome these problems we applied a multidisciplinary approach combining petrology and biostratigraphy on crustal remnants of the Neotethys incorporated into the mélange complexes of the Izmir–Ankara–Erzincan Suture Belt (IAESB).

As previously referred to, the location, age and geological evolution of the branch(es) of the Eastern Neotethys are disputed. In fact, most authors favour the hypothesis (presented herein) that implies the existence of two parallel and contemporaneous oceans, namely, the Izmir–Ankara Ocean, to the south, and the Intra-Pontide Ocean, to the north (see Göncüoglu *et al.* 2012 for an exhaustive review). In contrast, other authors favour the hypothesis that implies

†Author for correspondence: marco.chiari@unifi.it

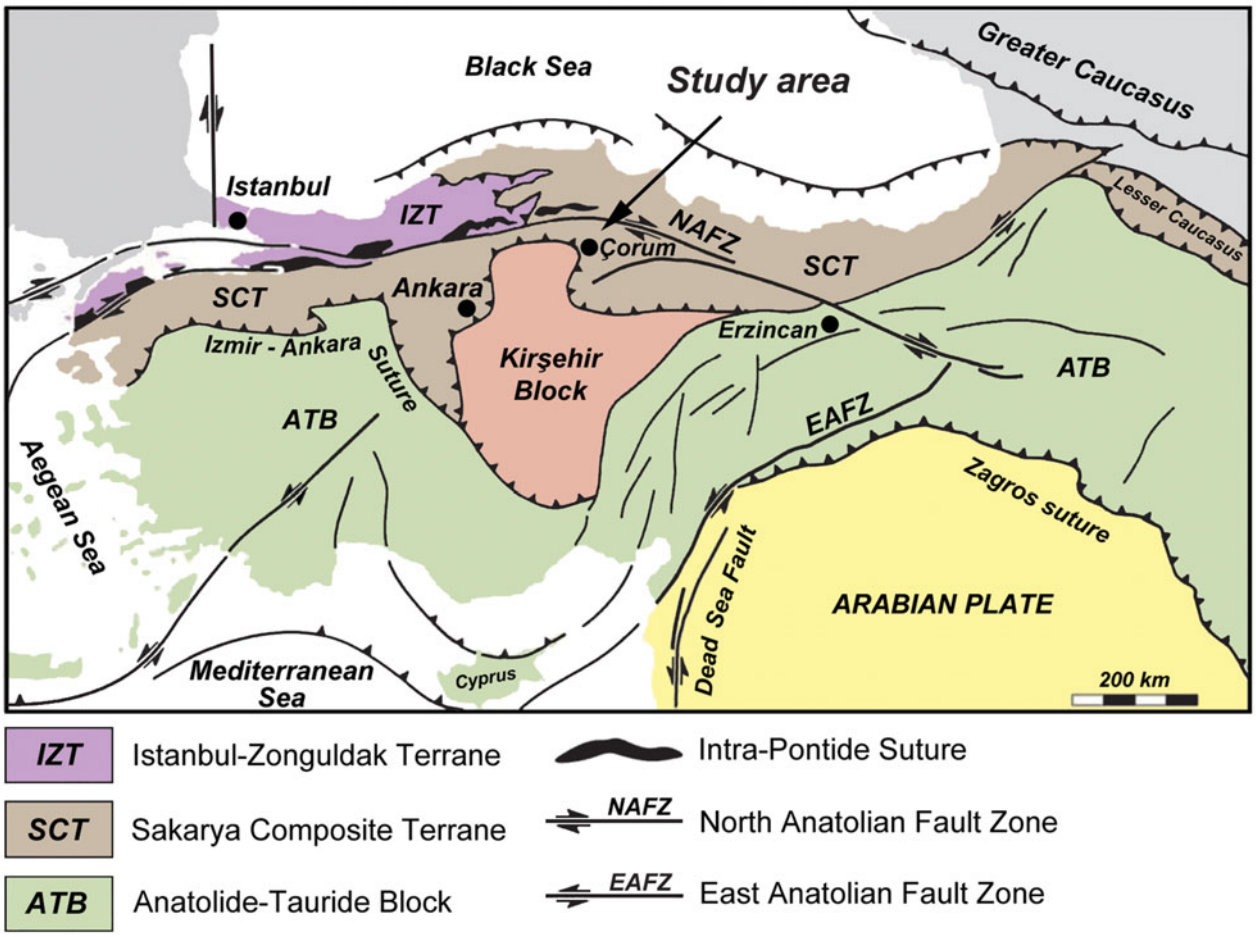

Figure 1. (Colour online) The main tectonic zones of Turkey (modified after Sengör & Yılmaz, 1981; Göncüoglu *et al.* 2012, modified).

the existence of a single oceanic basin represented by the Intra-Pontide Ocean (e.g. Bortolotti & Principi, 2005). In this case the Intra-Pontide Suture (IPS, see below) would be the eastward continuation of the Vardar Ocean suture, whereas the IAESB would represent fragments of the oceanic lithosphere pushed southwards onto the continent by orogenic movements (as happened more westwards, in the Hellenides) (see Saccani *et al*. 2008*a*; Bortolotti *et al.* 2013*b*).

The IAESB separates two completely different units of continental crust with different origins: (a) the Tauride–Anatolide terrane representing the rifted northern margin of NW Gondwana, in the south, and (b) the Sakarya Composite Terrane comprising amalgamated oceanic and continental bodies of Variscan and Cimmerian origin and their alpine platform, in the north. To the north of the Sakarya Composite Terrane another suture, the IPS, represents the boundary towards the Eurasian Istanbul–Zonguldak terrane (Fig. 1).

The IAESB represents remnants of the Vardar–Izmir–Ankara–Erzincan–Lesser Caucasus Ocean in Turkey. This ocean is considered the main northern branch of the Neotethys, whereas the Intra-Pontide oceanic basin to the north of it is a matter of debate (see above and, for a brief discussion, Göncüoglu *et al.* 2012 and Tekin *et al.* 2012). In NW Turkey, the IPS is clearly delineated by the presence of ophiolitic melanges between the Sakarya and the Istanbul–Zonguldak continental plates (e.g. Robertson & Ustaömer, 2004; Göncüoglu *et al.* 2008; Akbayram, Okay & Satir, 2012). By the wedging out of the Sakarya Composite Terrane in northern Central Anatolia, however, the IPS belt juxtaposes with the IAESB along splays of the North Anatolian Shear Zone (e.g. Ellero *et al.* 2015*a*) and the neotectonic strike-slip system generated owing to the Tertiary indentation and anticlockwise rotation of the Kırşehir Block (e.g. Cemen *et al.* 1993; Kaymakci *et al.* 2003). Towards the east and in NE Anatolia, the IAESB is again in its accustomed position between the Anatolides and the units of the Sakarya Composite Terrane (Topuz *et al.* 2013*a*,*b*; Parlak *et al.* 2013; Robertson *et al.* 2013). The vanishing of the IPS belt in the Central Pontides by the North Anatolian Shear Zone during the neotectonic period led some authors to completely ignore the IPS and hence the presence of an oceanic basin (e.g. Elmas & Yiğitbaş, 2001, 2005).

The IAESB is composed of a number S-verging tectonic slices or giant slide blocks representing (1)

incomplete sequences of various portions of the Izmir–Ankara–Erzincan oceanic lithosphere (e.g. Floyd *et al.* 2000; Göncüoglu *et al.* 2000; Göncüoglu, 2011); (2) an accretionary prism, known as the 'Ankara Mélange' (Bailey & McCallien, 1953) including blocks derived from different parts of the oceanic basin; (3) imbricated slices of successions formed in a foredeep basin associated with the emplacement of the oceanic material onto the Tauride–Anatolide passive margin.

This study is focused on slide blocks including oceanic lavas associated with pelagic sediments within the accretionary prism and the foredeep basin successions in the eastern part of the Ankara Mélange (for the preliminary data see Bortolotti *et al.* 2013*a*). This paper aims to draw a more comprehensive picture of the different basaltic rock types erupted in the Neotethys from Middle Jurassic to Early Cretaceous times. To this purpose, a detailed petrological and geochemical characterization of the volcanic rocks and a detailed biochronological investigation of the associated radiolarian cherts will be carried out. Similar multidisciplinary studies were applied to other parts of the IAESB between the Aegean coast and the western part of the Ankara Mélange (e.g. Bragin & Tekin, 1996; Yaliniz, Göncüoglu & Floyd, 2000; Göncüoglu, Tekin & Turhan, 2001; Rojay, Yaliniz & Altiner, 2001; Tekin, Göncüoglu & Turhan, 2002; Gökten & Floyd, 2007; Tekin & Göncüoglu, 2007, 2009; Göncüoglu *et al.* 2008; Göncüoglu, Sayit & Tekin, 2010; Tekin *et al.* 2012; Moix & Goričan, 2013; Göncüoglu *et al.* 2015; Soycan, Erdoğan & Konak, 2015). These studies reported Middle Triassic to Cretaceous ages for radiolarian cherts stratigraphically associated with basalts showing, in turn, different tectonomagmatic settings of formation, such as mid-ocean ridge, seamount, forearc and back-arc. Our new data from the eastern Ankara Mélange aim to interpret the tectonomagmatic processes and their timing, which will be useful for improving the reconstruction of the geodynamic history of the Neotethys Ocean mainly spanning the Jurassic to Early Cretaceous time interval.

2. Geological background

The studied portion of the IAESB was characterized by the pre-Eocene development of a huge accretionary prism (for details see Rojay, 2013), which formed between the Sakarya Composite Terrane to the north and the southerly Kütahya–Bolkardag Belt of the Anatolides, in the western part, and the Central Anatolian Crystalline Complex (CACC), in the eastern part. The first juxtaposition of these oceanic and continental units occurred in latest Cretaceous – Paleocene time. However, compression and related thrusting lasted until Miocene time (Kocyigit *et al.* 1995).

We sampled some ophiolitic outcrops from the IAESB east of Ankara (Fig. 1), where the concave E–W trend of the belt between Izmir and Ankara makes a sharp turn towards the NNW, caused by the Tertiary indentation (e.g. Cemen *et al.* 1993; Kaymakci *et al.* 2003) and anticlockwise rotation of the Kırşehir Block.

The Sakarya Unit marks the active margin of the Izmir–Ankara–Erzincan Ocean, and was thrust over the IAESB both to the NNE of Ankara and to the SE of Çorum (Fig. 2). It consists of a composite terrane comprising a Variscan arc complex and its Permian platform, as well as the Palaeotethyan subduction–accretion prism (the Triassic Karakaya Complex; Göncüoglu *et al.* 2000; Okay & Göncüoglu, 2004). It has a Jurassic to ?Upper Cretaceous cover that belonged to a N-facing passive continental margin but was transformed into an active margin by the northward subduction of the Izmir–Ankara–Erzincan oceanic lithosphere.

The Karakaya Complex NNW of Ankara comprises low-grade metamorphic greywackes associated with Permian and Carboniferous limestone blocks and ocean-island-type volcanic rocks with Carnian radiolarian cherts (e.g. Sayit, Tekin & Göncüoglu, 2011). Unconformably overlying them there is a Mesozoic cover that comprises, from bottom to top, upper Lower Jurassic – Middle Jurassic neritic limestones, Upper Jurassic – Lower Cretaceous (e.g. Altiner *et al.* 1991) pelagic limestones and Upper Cretaceous turbidites. The oldest common overstep sequence on the IAESB (and the Sakarya Composite Terrane) comprises Upper Paleocene lagoonal sediments, which occur as discontinuous outcrops within the thrust zone between these two units (Göncüoglu *et al.* 2000).

The northern-central part of the sampled area has been recently evaluated as the North Anatolian Shear Zone (Ellero *et al.* 2015*a*,*b*). The North Anatolian Shear Zone corresponds to a complex deformation zone where the strain is partitioned in a system of faults, folds and thrusts leading to high-angle faults bounding E–W-elongated blocks and pull-apart basins. The zone is more than 100 km wide and comprises several kilometres long, lens-shaped tectonic inlayers belonging to the mélanges of the IPS belt (e.g. Göncüoglu *et al.* 2014), the Sakarya Composite Terrane (mainly the Upper Jurassic – Lower Cretaceous Sogukcam Limestone, e.g. Catanzariti *et al.* 2013), a Late Cretaceous island arc (Berber, Göncüoglu & Sayit, 2014) belonging to the IPS belt, a Late Cretaceous continental arc (Ellero *et al.* 2015*b*) and the ophiolitic mélanges of the IAESB. The active main strand of the right-lateral North Anatolian Transform Fault is located in the centre of this megashear zone, where lateral displacements ranging from 30 to 120 km have been proposed in the literature (e.g. Hubert-Ferrari *et al.* 2002 and references therein).

The metamorphic rocks of the Sakarya Composite Terrane (the 'Tokat Massif', Yilmaz *et al.* 1997), around Çorum, east of the sampled area (Fig. 2), are tectonically overlying the ophiolitic mélange of the IAESB. In this area, both units are in turn unconformably overlain by Middle Eocene rocks. Unfortunately, the primary relations between the Sakarya and IAESB

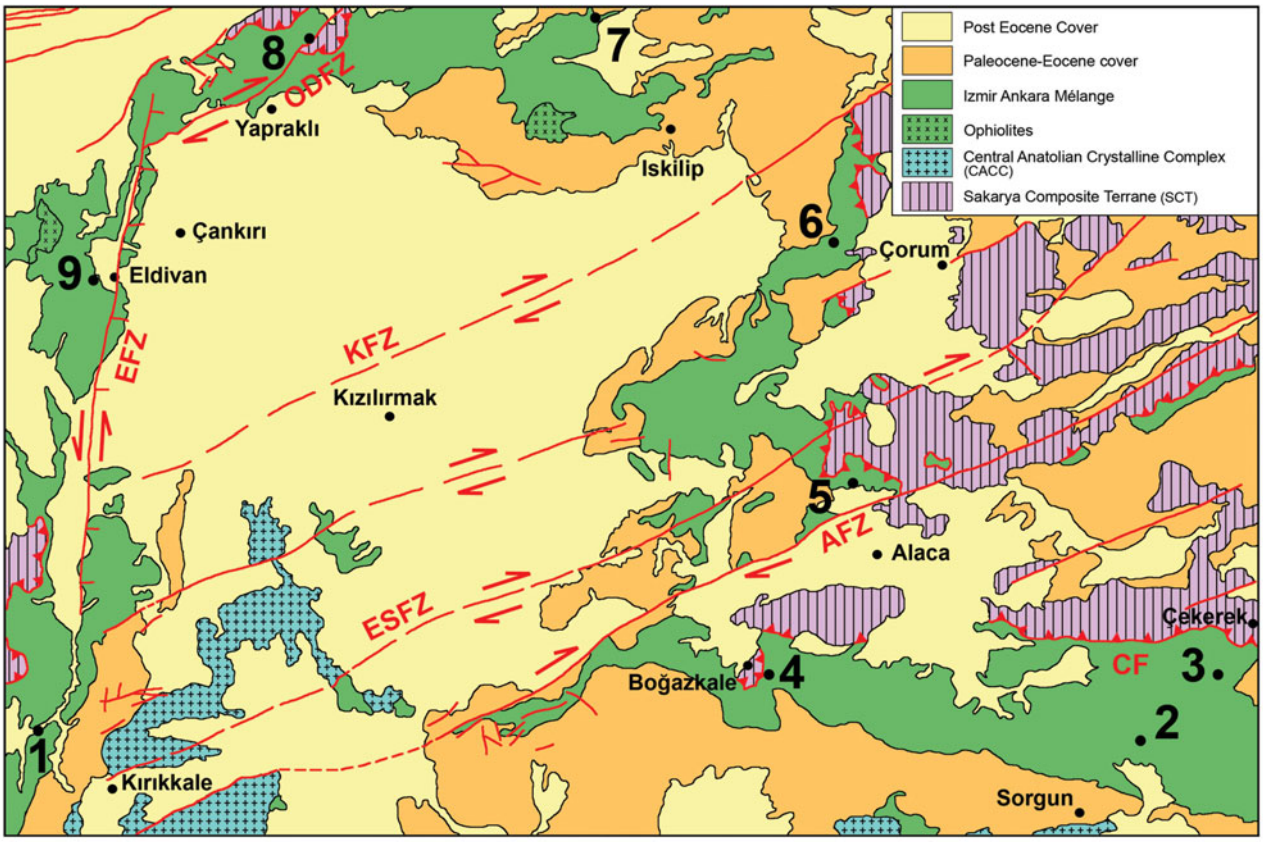

Figure 2. (Colour online) Sketch geological map of the study area, with the location of the sampled sections (after Bortolotti *et al.* 2013*a*, modified and Yolsal-Çevikbilen *et al.* 2012). EFZ – Eldivan Fault Zone; ODFZ – Orta–Devrez Fault Zone; KFZ – Kızılırmak Fault Zone; ESFZ – Ezine Pazarı–Sungurlu Fault Zone; AFZ – Alaca Fault Zone; CF – Çekerek Fault.

rocks are obscured by intensive Oligocene strike-slip faulting (Fig. 2).

Structurally underlying the IAESB units, the continental crust that was palinspastically located to the south, and west of Ankara, represents the northern rim of the Tauride–Anatolide Platform. It mainly includes high-pressure–low-temperature metamorphosed tectonic slices (e.g. Okay & Tüysüz, 1999) whose lithostratigraphic sequences are similar to the Palaeozoic–Mesozoic slope-type successions of the Anatolides (Göncüoglu, 2011). In particular, in the sampled area (Fig. 2), the IAESB units were thrust onto the CACC (Yaliniz, Floyd & Göncüoglu, 1996; Yaliniz, Göncüoglu & Özkan-Altiner, 2000), which comprises high-temperature–medium-pressure metamorphic successions similar to the Palaeozoic–Mesozoic Tauride–Anatolide Platform. In turn, they were overthrust by Turonian supra-subduction ophiolites: the Central Anatolian Ophiolites (Yaliniz, Göncüoglu & Floyd, 2000), which represent remnants of the Izmir–Ankara–Erzincan Ocean. Late Campanian granitoids intrude both the basement rocks and the overlying ophiolite units (Köksal & Göncüoglu, 2008), indicating a Late Cretaceous age for the inception of obduction. The oldest overstep sequences in this area are again post-Maastrichtian pre-Lower Eocene (Gülyüz *et al.* 2013) red conglomerates, testifying to a Paleocene age for the main juxtaposition of the CACC and IAESB mélanges.

In the central part of the sampled area, the IAESB rocks are covered by the Paleocene–Eocene post-orogenic marine clastic-volcaniclastic rocks, carbonates and volcanic rocks of the Çankırı Basin, which, in turn, are partly covered by Neogene sediments (e.g. Göncüoglu, 1992). Within the basin the anticlockwise rotation of the CACC induced the formation of several NE–SW-trending right-lateral faults and, at its western margin, important left-lateral faults (Fig. 2). When restored, the IAESB palinspastically follows also a roughly E–W trend and the present distortion of the main tectonic units is re-established.

To attempt a reconstruction of the thickness of the IAESB rocks that compose the subducted and accreted remnants of the Izmir–Ankara–Erzincan oceanic lithosphere, together with island arc and sedimentary rocks of several Late Cretaceous – Paleocene piggy-back basins (e.g. Cater *et al.* 1991; Erdogan, Akay & Ugur, 1996), geophysical data would be necessary, but at present these date are not available.

3. Description of the sampled sections

All the sampled sequences pertain to the radiolarite–basalt blocks included in the Ankara Mélange. For the

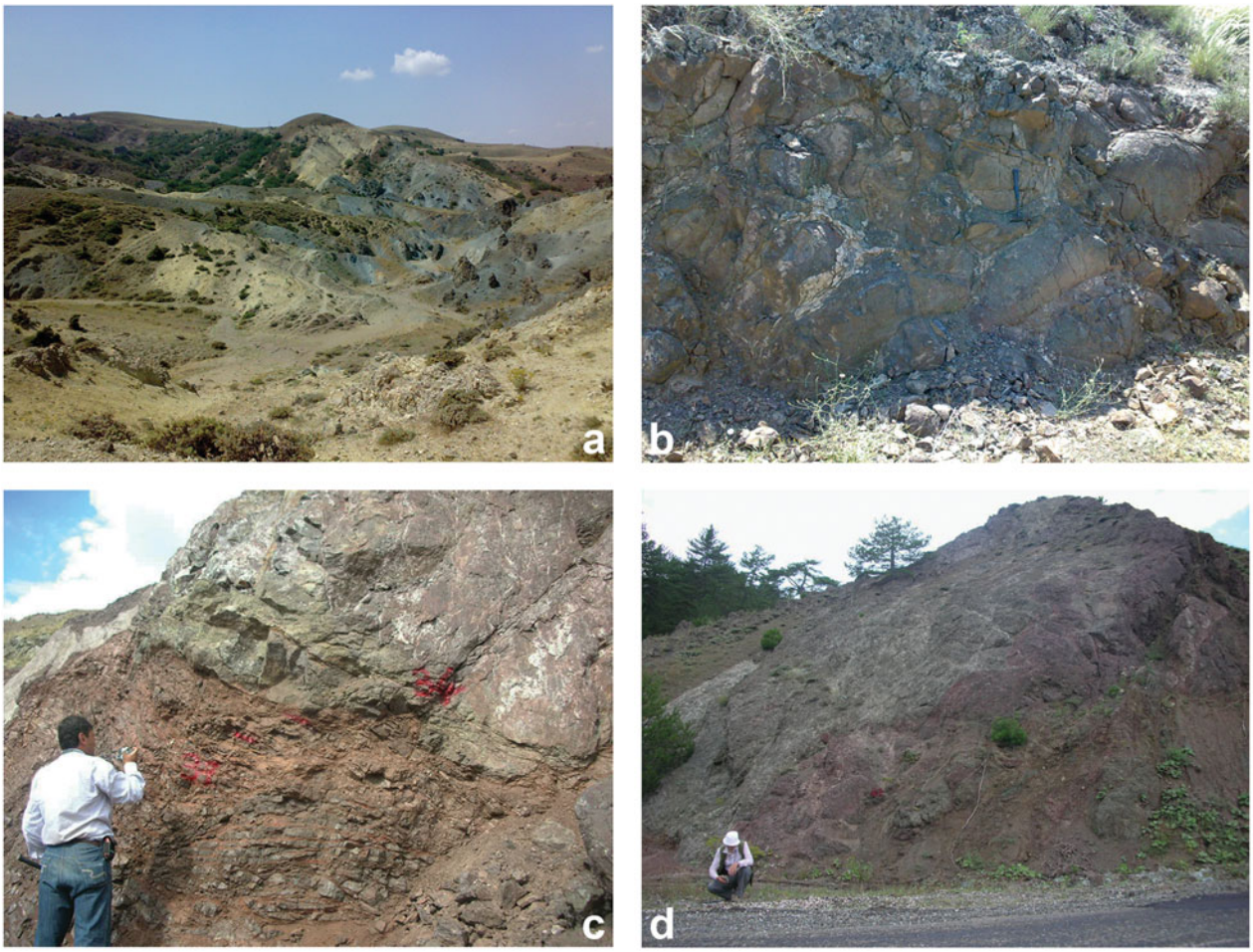

Figure 3. (Colour online) (a) Serpentinite mélange near Beynam. (b) Pillow basalts along the road from Elmadag to Kırıkkale (Section 1). Length of hammer for scale is 32 cm. (c) Overturned sequence of basalts and radiolarian cherts along the road from Çorum to Alaca (Section 5). (d) Outcrop of basalts and radiolarian cherts along the road from Iskilip to Tosya (Section 7). Modified from Bortolotti *et al.* (2013*a*).

numbering of the sections we referred to Bortolotti *et al.* (2013*a*). It is worth noting that in the present paper we do not report the samples from Section 6 of Late Triassic age of Bortolotti *et al.* (2013*a*).

3.a. Section 1

In a massif of pillow basalts along the Elmadag–Kırıkkale road, several metric intercalations of siliceous shales with scattered radiolarian cherts crop out.

We sampled one of these intercalations and the associated basalts (Fig. 3b, 39° 55.023′ N, 33° 21.989′ E).

Samples: TU10.4, radiolarian chert; TU10.6, TU10.10, basalts below the radiolarian chert intercalation; TU10.9, basalt ~20 m above the radiolarian chert intercalation.

3.b. Section 2

In a massif of mainly pillow basalts along the Sorgun–Çekerek road, thin layers of radiolarian cherts crop out.

We sampled one of these layers and the associated basalts (39° 54.889′ N, 35° 18.063′ E); one radiolarian chert sample was collected along the road in an uncertain stratigraphic position.

Samples: TU10.11, radiolarian chert with uncertain stratigraphic position; TU10.12, radiolarian chert; TU10.14 basalt at the contact with the radiolarites; TU10.15, TU10.16, TU10.17, basalts collected several metres from the radiolarites.

3.c. Section 3

In a basalt block immediately north of Gökdere village, along the road, a sequence with radiolarian cherts crops out.

Samples: TU10.19, basalt at the contact with the radiolarian cherts (39° 59.924′ N, 35° 24.272′ E); TU10.22, TU10.23, basalts collected some metres southwards (39° 59.921′ N, 35° 24.274′ E), respectively 3.5 and 2 m from the contact with the radiolarites; TU10.28, radiolarian chert collected ~22 m from the basalts (this sequence is intensely folded).

3.d. Section 4

An overturned sequence of basalts and radiolarian cherts with a sheared contact, along the road

~3 km southeast of Bogazkale (40° 00.377′ N, 34° 38.762′ E).

Samples: TU10.29, TU10.30, TU10.31, radiolarian cherts collected ~20 cm above the sheared level; 60 cm of sheared argillites and cherts separates the basalts from the above samples; TU10.32, basalt at the contact with the sheared level; TU10.33, basalt collected some metres above.

3.e. Section 5

Big quarry cut by small faults that pull the contact between the basalts–cherts up and down. The sequence could be overturned: the cherts lie under the basalts; the contact is very clear with pockets of argillites and cherts in the mainly massif basalts. The sampled quarry is along the Çorum to Alaca road, south of Küre village (Fig. 3c, 40° 15.861′ N, 34° 48.187′ E).

Samples: TU10.34, basalt, sample collected ~6 m from the cherts; TU10.35, TU10.36, TU10.37, samples collected in a radiolarian chert–argillite sequence from the base to 40 cm up. A small normal fault shifts the sequence by some metres. TU10.38, radiolarian chert, collected beyond the fault, ~30 cm from the basalt sample TU10.40; TU10.40, basalt at the contact with the radiolarian cherts; TU10.39, basalt nearby sample TU10.40.

3.f. Section 7

Small outcrop of basalts and cherts along the Iskilip–Tosya road, 1.2 km before the junction to Hacihalil village (Fig. 3d, 40° 53.378′ N, 34° 20.756′ E).

Samples: TU10.45, radiolarian chert nodule in the basalts; TU10.46, basalt.

3.g. Section 8

Large body of breccia(?) with basalts, microgabbros, serpentinites and crystallized limestones in a cherty matrix. We sampled the breccia in two close localities northeast of Yukariöz village.

Samples: First locality (40° 51.097′ N, 33° 50.723′ E), TU10.47, TU10.48, radiolarian cherts; TU10.49a, TU10.49b, basalts. Second locality (40° 51.527′ N, 33° 49.577′ E), TU10.51, M10 radiolarian cherts.

3.h. Section 9

Pillow basalts enveloped in reddish limestones, Eldivan–Sabanozu road (40° 31.488′ N, 33° 28.106′ E).

Samples: TU10.52, TU10.53, basalts; TU10.54, TU10.55, limestones.

4. Biostratigraphy

The radiolarian samples were etched with hydrochloric and hydrofluoric acid following the method proposed by Dumitrica (1970), Pessagno & Newport (1972), Baumgartner *et al.* (1981) and De Wever (1982). The examined samples yielded radiolarians with moderate preservation and the principal marker taxa are illustrated in Figures 4 and 5.

For the taxonomy and ranges of the Late Jurassic – Early Cretaceous principal marker taxa we refer to Aliev (1967), Kozur (1985), Kawabata (1988), Aita & Okada (1986), Goričan (1994), O'Dogherty (1994), Baumgartner *et al.* (1995*a*,*b*), Dumitrica & Dumitrica-Jud (1995), Bak (1996, 1999), Dumitrica, Immenhauser & Dumitrica-Jud (1997), Chiari, Marcucci & Prela (2004), Danelian *et al.* (2004), Smuc & Goričan (2005), Filippov & Kemkin (2005), Chiari, Cobianchi & Picotti (2007), Danelian (2008), Dumitrica & Zügel (2008), O'Dogherty *et al.* (2009), Robin *et al.* (2010), Bandini *et al.* (2011), Goričan, Pavšič & Rožič (2012) and Chiari *et al.* (2012).

From the analysed cherts the following radiolarian assemblages and ages were obtained:

4.a. Section 1

TU10.4. Angulobracchia portmanni Baumgartner, *Archaeodictyomitra mitra* Dumitrica, *Archaeodictyomitra* sp. cf. *A. lacrimula* (Foreman) (Fig. 4a), *Archaeodictyomitra* sp. cf. *A. mitra* Dumitrica, *Archaeodictyomitra* sp., *Archaeodictyomitra* (?) sp., *Aurisaturnalis variabilis variabilis* (Squinabol) (Fig. 4b), *Hemicryptocapsa* sp. cf. *H. capita* Tan (Fig. 4c), *Neorelumbra* (?) sp., *Pseudodictyomitra* sp., *Pseudodictyomitra* (?) sp., *Pyramispongia* (?) sp., *Tethysetta* (?) sp., *Thanarla brouweri* (Tan) (Fig. 4d), *Thanarla* sp., *Torculum* (?) sp., *Xitus* sp. cf. *X. robustus* Wu, *Xitus* sp.

Age. Late Valanginian to late Hauterivian (UAZ. 17–20; UAZones after Baumgartner *et al.* 1995*a*) based on the presence of *Aurisaturnalis variabilis variabilis* (Squinabol). Ranges after Baumgartner *et al.* (1995*b*).

4.b. Section 2

TU10.11. Eoxitus (?) sp. (Fig. 4e), *Praewilliriedellum* sp. cf. *P. japonicum* (Yao), *Stichomitra* (?) *takanoensis* Aita (Fig. 4f), *Striatojaponocapsa* (?) sp.

Age. Early–middle Bajocian to late Bathonian–early Callovian (UAZ. 3–7; UAZones after Baumgartner *et al.* 1995*a*) based on the presence of *Stichomitra* (?) *takanoensis* Aita. Range after Baumgartner *et al.* (1995*b*).

TU10.12. Hiscocaspsa sp. (Fig. 4g), *Mirifusus* sp. cf. *M. guadalupensis* Pessagno (Fig. 4h), *Parahsuum* sp., *Parahsuum* (?) sp., *Praewilliriedellum* sp. cf. *P. japonicum* (Yao), *Praewilliriedellum* (?) sp., *Pseudodictyomitra* (?) sp., *Stichomitra* (?) *takanoensis* Aita (Fig. 4i), *Transhsuum* sp., *Transhsuum* (?) sp., *Tritrabs* (?) sp.

Age. Early–middle Bajocian to late Bathonian–early Callovian (UAZ. 3–7; UAZones after Baumgartner *et al.* 1995*a*) based on the presence of *Stichomitra*

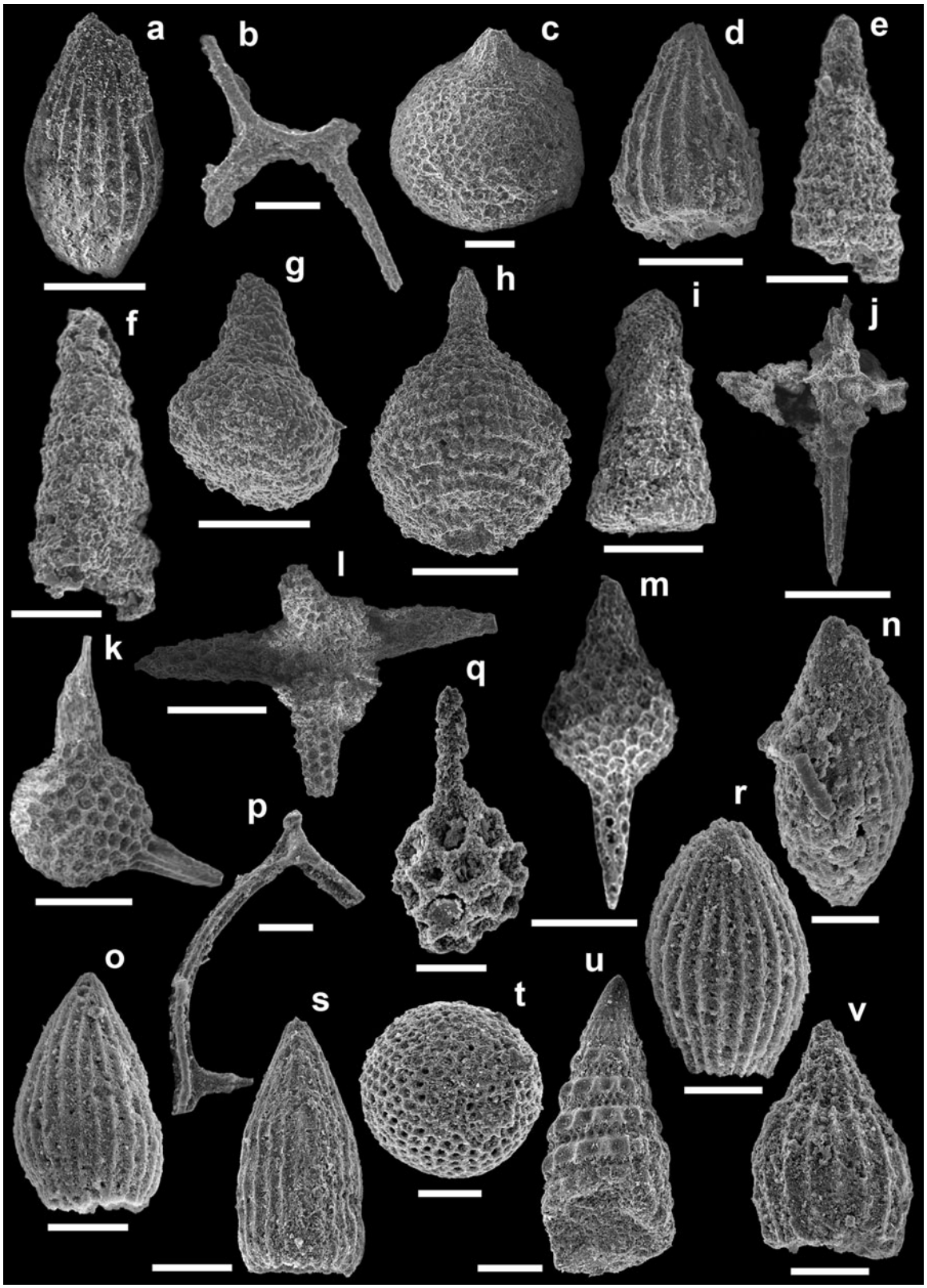

Figure 4. **S**cale bar = 50 μm. (a) *Archaeodictyomitra* sp. cf. *A. lacrimula* (Foreman), Section 1, TU10.4; (b) *Aurisaturnalis variabilis variabilis* (Squinabol), Section 1, TU10.4; (c) *Hemicryptocapsa* sp. cf. *H. capita* Tan, Section 1, TU10.4; (d) *Thanarla brouweri* (Tan), Section 1, TU10.4; (e) *Eoxitus* (?) sp., Section 2, TU10.11; (f) *Stichomitra* (?) *takanoensis* Aita, Section 2, TU10.11; (g) *Hiscocapsa* sp. Section 2, TU10.12; (h) *Mirifusus* sp. cf. *M. guadalupensis* Pessagno, Section 2, TU10.12; (i) *Stichomitra* (?) *takanoensis* Aita, Section 2, TU10.12; (j) *Emiluvia* sp. cf. *E. ordinaria* Ozvoldova, Section 3, TU10.28; (k) *Fultacapsa sphaerica* (Ozvoldova), Section 3, TU10.28; (l) *Podocapsa amphitreptera* Foreman, Section 3, TU10.28; (m) *Spinosicapsa* (?) sp., Section 3, TU10.28; (n) *Archaeodictyomitra lacrimula* (Foreman), Section 4, TU10.29; (o) *Archaeodictyomitra mitra* Dumitrica, Section 4, TU10.29; (p) *Dicerosaturnalis trizonalis* (Rüst), Section 4, TU10.29; (q) *Pantanellium* sp. cf. *P. squinaboli* (Tan), Section 4, TU10.29; (r) *Thanarla* sp. cf. *T. gutta* Jud, Section 4, TU10.29; (s) *Archaeodictyomitra* sp., Section 4, TU10.30; (t) *Holocryptocanium barbui* Dumitrica, Section 4, TU10.30; (u) *Pseudodictyomitra lanceloti* Schaaf, Section 4, TU10.30; (v) *Thanarla* sp. cf. *T. pacifica* Nakaseko & Nishimura, Section 4, TU10.30.

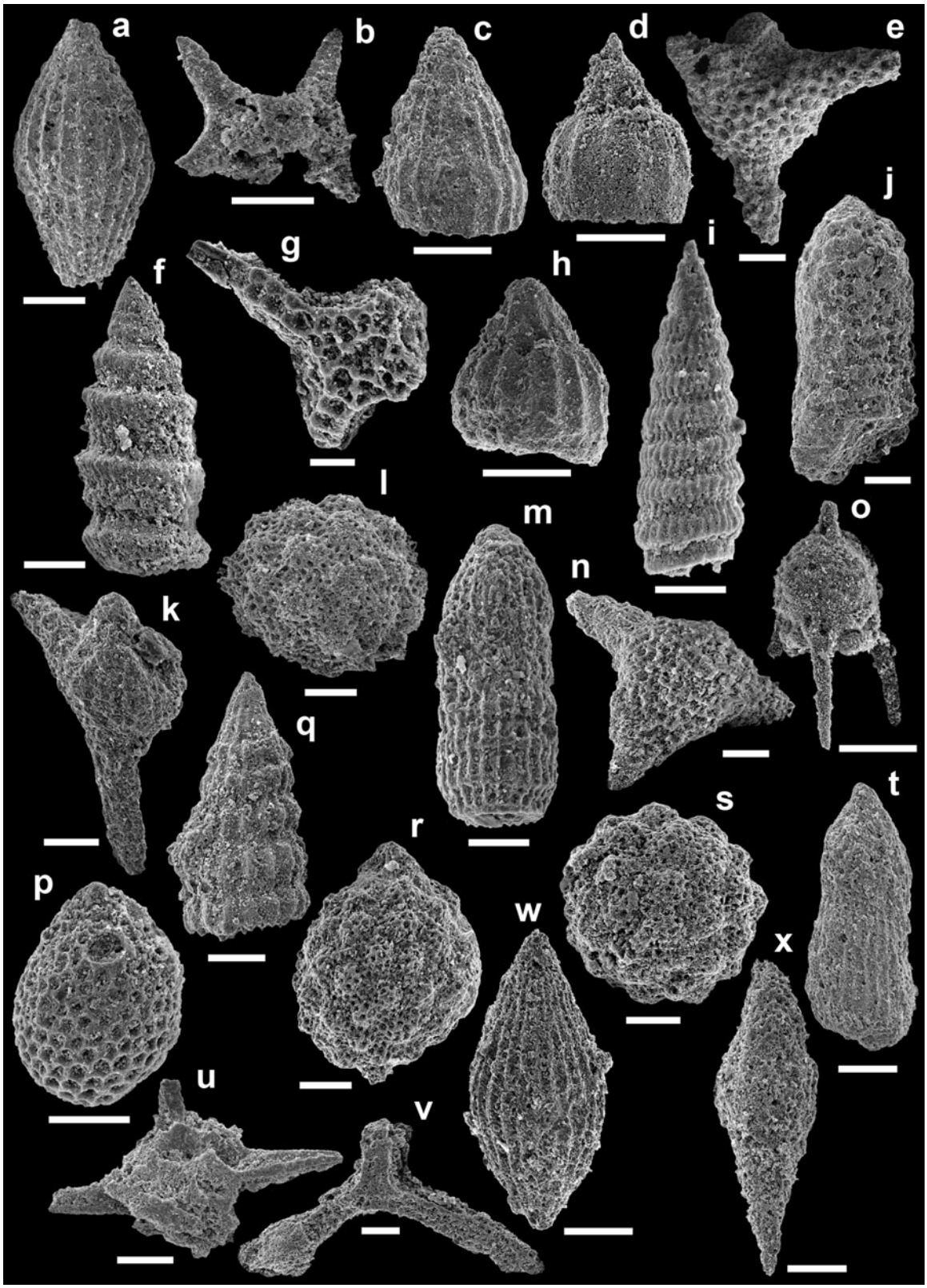

Figure 5. Scale bar = 50 μm. (a) *Archaeodictyomitra lacrimula* (Foreman), Section 4, TU10.31; (b) *Aurisaturnalis carinatus perforatus* Dumitrica & Dumitrica-Jud, Section 4, TU10.31; (c) *Thanarla brouweri* (Tan), Section 4, TU10.31; (d) *Eucyrtidiellum pyramis* (Aita), Section 5, TU10.35; (e) *Podocapsa amphitreptera* Foreman, Section 5, TU10.35; (f) *Cinguloturris cylindra* Kemkin & Rudenko, Section 5, TU10.36; (g) *Emiluvia* sp. cf. *E. ordinaria* Ozvoldova, Section 5, TU10.36; (h) *Eucyrtidiellum pyramis* (Aita), Section 5, TU10.36; (i) *Loopus primitivus* (Matsuoka & Yao), Section 5, TU10.36; (j) *Ristola cretacea* (Baumgartner), Section 5, TU10.36; (k) *Podocapsa amphitreptera* Foreman, Section 5, TU10.37; (l) *Praeconosphaera* (?) *sphaeroconus* (Rüst), Section 5, TU10.37; (m) *Archaeodictyomitra* sp. cf. *A. excellens* (Tan), Section 5, TU10.38; (n) *Podocapsa amphitreptera* Foreman, Section 5, TU10.38; (o) *Saitoum* sp. cf. *S. elegans* De Wever, Section 5, TU10.38; (p) *Zhamoidellum ovum* Dumitrica, Section 5, TU10.38; (q) *Archaeodictyomitra* sp. cf. *A. coniforma* Dumitrica, Section 7, TU10.45; (r) *Cryptamphorella clivosa* (Aliev), Section 7, TU10.45; (s) *Praeconosphaera* (?) *sphaeroconus* (Rüst), Section 7, TU10.45; (t) *Archaeodictyomitra excellens* (Tan), Section 8, TU10.47; (u) *Cana septemporatus* (Parona), Section 8, TU10.47; (v) *Halesium* sp. cf. *H. palmatum* Dumitrica, Section 8, TU10.47; (w) *Archaeodictyomitra lacrimula* (Foreman), Section 8, TU10.51; (x) *Pseudoeucyrtis* sp. cf. *P. hanni* (Tan) *sensu* O'Dogherty (1994), Section 8, TU10.51.

(?) *takanoensis* Aita. Range after Baumgartner *et al.* (1995*b*).

4.c. Section 3

TU.10.28. Acaeniotylopsis sp., *Crolanium* (?) sp., *Emiluvia* sp. cf. *E. ordinaria* Ozvoldova (Fig. 4j), *Eoxitus* (?) sp., *Fultacapsa sphaerica* (Ozvoldova) (Fig. 4k), *Mirifusus* sp. cf. *M. guadalupensis* Pessagno, *Mirifusus* sp., *Podocapsa amphitreptera* Foreman (Fig. 4l), *Spinosicapsa* sp. cf. *S. triacantha* (Fischli), *Spinosicapsa* (?) sp. (Fig. 4m), *Spongocapsula* sp., *Svinitzium* sp., *Svinitzium* (?) sp., *Triactoma* (?) sp.

Age. Middle–late Oxfordian to late Kimmeridgian–early Tithonian (UAZ. 9–11; UAZones after Baumgartner *et al.* 1995*a*) based on the occurrence of *Podocapsa amphitreptera* Foreman with *Fultacapsa sphaerica* (Ozvoldova). Ranges after Baumgartner *et al.* (1995*b*).

4.d. Section 4

TU10.29. Archaeodictyomitra lacrimula (Foreman) (Fig. 4n), *Archaeodictyomitra mitra* Dumitrica (Fig. 4o), *Archaeodictyomitra* sp., *Dicerosaturnalis trizonalis* (Rüst) (Fig. 4p), *Holocryptocanium* sp. cf. *H. barbui* Dumitrica, *Orbiculiformella* (?) sp., *Pantanellium* sp. cf. *P. squinaboli* (Tan) (Fig. 4q), *Praeconosphaera* (?) sp. cf. *P.* (?) *multiconus* Yang, *Praeconosphaera* (?) sp., *Praewilliriedellum* sp. cf. *P. japonicum* (Yao), *Pseudoeucyrtis* sp., *Thanarla brouweri* (Tan) *sensu* O'Dogherty (1994), *Thanarla* sp. cf. *T. gutta* Jud (Fig. 4r), *Thanarla* sp.

Age. Early–early late Berriasian to middle Aptian–early Albian (UAZ. 14 – *Costata* Subzone of *Turbocapsula* Zone; zone after O'Dogherty, 1994; UAZone after Baumgartner *et al.* 1995*a*) based on the occurrence of *Archaeodictyomitra lacrimula* (Foreman) and *Archaeodictyomitra mitra* Dumitrica. Ranges after Baumgartner *et al.* (1995*b*), O'Dogherty (1994), Dumitrica, Immenhauser & Dumitrica-Jud (1997) and Bandini *et al.* (2011).

TU10.30. Archaeodictyomitra sp. cf. *A. communis* (Squinabol), *Archaeodictyomitra* sp. cf. *A. lacrimula* (Foreman), *Archaeodictyomitra* sp. (Fig. 4s), *Archaeodictyomitra* (?) sp., *Emiluvia* (?) sp., *Eoxitus* sp., *Hiscocapsa* (?) sp., *Holocryptocanium barbui* Dumitrica (Fig. 4t), *Holocryptocanium* sp. cf. *H. barbui* Dumitrica, *Pantanellium* sp., *Praeconosphaera* (?) sp., *Pseudodictyomitra lanceloti* Schaaf (Fig. 4u), *Pseudodictyomitra* sp. cf. *P. lanceloti* Schaaf, *Thanarla* sp. aff. *T. brouweri* (Tan), *Thanarla* sp. cf. *T. pacifica* Nakaseko & Nishimura (Fig. 4v), *Thanarla* sp. cf. *T. praeveneta* Pessagno, *Thanarla* sp., *Thanarla* (?) sp.

Age. Late Hauterivian to middle Aptian–early Albian (UAZ. 20 – *Costata* Subzone of *Turbocapsula* Zone; zone after O'Dogherty, 1994; UAZone after Baumgartner *et al.* 1995*a*) based on the presence of *Pseudodictyomitra lanceloti* Schaaf. Range after Baumgartner *et al.* (1995*b*) and Bandini *et al.* (2011).

TU10.31. Angulobracchia (?) sp., *Archaeodictyomitra lacrimula* (Foreman) (Fig. 5a), *Archaeodictyomitra mitra* Dumitrica, *Archaeodictyomitra* sp. cf. *A. lacrimula* (Foreman), *Archaeodictyomitra* sp., *Aurisaturnalis carinatus perforatus* Dumitrica & Dumitrica-Jud (Fig. 5b), *Dicerosaturnalis trizonalis* (Rüst), *Halesium* (?) sp., *Pantanellium* sp., *Praeconosphaera* (?) sp. cf. *P.* (?) *multiconus* Yang, *Praeconosphaera* (?) sp., *Praexitus* sp., *Pseudodictyomitra lanceloti* Schaaf, *Pseudodictyomitra* sp. cf. *P. lanceloti* Schaaf, *Pseudodictyomitra* sp., *Pseudodictyomitra* (?) sp., *Spinosicapsa* (?) sp., *Thanarla brouweri* (Tan) (Fig. 5c), *Thanarla* sp. cf. *T. brouweri* (Tan), *Thanarla* sp. cf. *T. pacifica* Nakaseko & Nishimura, *Thanarla* sp. cf. *T. pulchra* (Squinabol), *Thanarla* sp., *Xitus* sp., *Xitus* (?) sp.

Age. Middle late Barremian–early early Aptian based on the occurrence of *Aurisaturnalis carinatus perforatus* Dumitrica & Dumitrica-Jud. Range after Dumitrica & Dumitrica-Jud (1995).

4.e. Section 5

TU10.35. Archaeodictyomitra (?) sp., *Dicerosaturnalis trizonalis* (Rüst), *Dicerosaturnalis* sp. cf. *D. trizonalis* (Rüst), *Emiluvia* sp. cf. *E. ultima* Baumgartner, *Emiluvia* sp., *Eucyrtidiellum pyramis* (Aita) (Fig. 5d), *Mirifusus* sp. cf. *M. dianae* (Karrer) s.l., *Mirifusus* sp., *Napora* sp., *Podocapsa amphitreptera* Foreman (Fig. 5e), *Praeconosphaera* (?) sp., *Pseudodictyomitra* (?) sp., *Spinosicapsa* (?) sp., *Svinitzium* (?) sp., *Syringocapsa* (?) sp., *Triactoma* sp. cf. *T. jonesi* (Pessagno), *Triactoma* (?) sp., *Zhamoidellum* (?) sp.

Age. Early–early late Tithonian to latest Tithonian–earliest Berriasian (UAZ. 12–13; UAZones after Baumgartner *et al.* 1995*a*) based on the presence of *Eucyrtidiellum pyramis* (Aita). Range after Baumgartner *et al.* (1995*b*).

TU10.36. Archaeodictyomitra apiarium (Rüst), *Archaeodictyomitra* sp. aff. *A. excellens* (Tan), *Archaeodictyomitra* sp. aff. *A. rigida* Pessagno, *Archaeodictyomitra* sp. cf. *A. apiarium* (Rüst), *Archaeodictyomitra* sp. 1, *Archaeodictyomitra* sp., *Cinguloturris cylindra* Kemkin & Rudenko (Fig. 5f), *Emiluvia* sp. cf. *E. ordinaria* Ozvoldova (Fig. 5g), *Emiluvia* sp. cf. *E. orea* Baumgartner, *Emiluvia* (?) sp., *Eucyrtidiellum pyramis* (Aita) (Fig. 5h), *Eucyrtidiellum* (?) sp. cf. *E.* (?) *quinatum* Takemura, *Loopus primitivus* (Matsuoka & Yao) (Fig. 5i), *Loopus* sp. cf. *L. doliolum* Dumitrica, *Mirifusus dianae* s.l. (Karrer), *Mirifusus* sp., *Olanda* sp., *Podocapsa amphitreptera* Foreman, *Praeconosphaera* (?) *sphaeroconus* (Rüst), *Praeconosphaera* (?) sp. cf. *P.* (?) *sphaeroconus* (Rüst), *Praeconosphaera* (?) sp., *Pseudodictyomitra* sp. cf. *P. carpatica* (Lozyniak), *Pseudodictyomitra* (?) sp., *Ristola cretacea* (Baumgartner) (Fig. 5j), *Ristola* (?) sp., *Sethocapsa horokanaiensis* Kawabata, *Syringocapsa* (?) sp., *Zhamoidellum* sp. cf. *Z.* sp. A *sensu* Goričan (1994), *Zhamoidellum* sp.

Age. Early–early late Tithonian (UAZ. 12; UAZone after Baumgartner *et al.* 1995*a*) based on the occurrence of *Cinguloturris cylindra* Kemkin & Rudenko, *Eucyrtidiellum pyramis* (Aita) and *Ristola cretacea* (Baumgartner) with *Loopus primitivus* (Matsuoka & Yao). Ranges after Baumgartner *et al.* (1995*b*).

TU10.37. Archaeodictyomitra (?) sp., *Podocapsa amphitreptera* Foreman (Fig. 5k), *Praeconosphaera* (?) *sphaeroconus* (Rüst) (Fig. 5l), *Pseudodictyomitra* (?) sp., *Spinosicapsa* (?) sp.

Age. Late Oxfordian–early Kimmeridgian to latest Valanginian–earliest Hauterivian (UAZ. 10–18; UAZones after Baumgartner *et al.* 1995*a*) based on the occurrence of *Praeconosphaera* (?) *sphaeroconus* (Rüst) with *Podocapsa amphitreptera* Foreman. Ranges after Baumgartner *et al.* (1995*b*), Chiari, Cobianchi & Picotti (2007) and Bandini *et al.* (2011).

TU10.38. Archaeodictyomitra sp. aff. *A. chalilovi* (Aliev), *Archaeodictyomitra* sp. aff. *A. excellens* (Tan), *Archaeodictyomitra* sp. aff. *A. ioniana* Danelian, *Archaeodictyomitra* sp. cf. *A. apiarium* (Rüst), *Archaeodictyomitra* sp. cf. *A. excellens* (Tan) (Fig. 5m), *Archaeodictyomitra* sp. cf. *A. minoensis* (Mizutani), *Archaeodictyomitra* sp., *Archaeodictyomitra* (?) sp., *Becus* (?) sp., *Cinguloturris* sp. cf. *C. carpatica* Dumitrica, *Dicerosaturnalis trizonalis* (Rüst), *Dicerosaturnalis* sp. cf. *D. trizonalis* (Rüst), *Emiluvia* sp., *Pantanellium* sp., *Podocapsa amphitreptera* Foreman (Fig. 5n), *Praeconosphaera* (?) sp., *Pseudodictyomitra* sp. cf. *P. thurowi* Dumitrica, *Pseudodictyomitra* sp., *Saitoum* sp. cf. *S. elegans* De Wever (Fig. 5o), *Saitoum* (?) sp., *Spinosicapsa* (?) sp., *Syringocapsa* (?) sp., *Zhamoidellum ovum* Dumitrica (Fig. 5p), *Zhamoidellum* sp.

Age. Middle–late Oxfordian to late Kimmeridgian–early Tithonian (UAZ. 9–11; UAZones after Baumgartner *et al.* 1995*a*) based on the presence of *Podocapsa amphitreptera* Foreman and *Zhamoidellum ovum* Dumitrica. Ranges after Baumgartner *et al.* (1995*b*) and Smuc & Goričan (2005).

4.f. Section 7

TU10.45. Archaeodictyomitra sp. cf. *A. communis* (Squinabol), *Archaeodictyomitra* sp. cf. *A. coniforma* Dumitrica (Fig. 5q), *Archaeodictyomitra* sp., *Archaeodictyomitra* (?) sp., *Cryptamphorella clivosa* (Aliev) (Fig. 5r), *Godia* sp. cf. *G. decora* (Li & Wu), *Godia* (?) sp., *Holocryptocanium* sp. cf. *H. barbui* Dumitrica, *Praeconosphaera* (?) *sphaeroconus* (Rüst) (Fig. 5s), *Praeconosphaera* (?) sp., *Pseudodictyomitra* (?) sp., *Tethysetta* sp. cf. *T. usotanensis* (Tumanda), *Thanarla brouweri* (Tan), *Thanarla* sp. cf. *T. pulchra* (Squinabol), *Thanarla* sp., *Thanarla* (?) sp.

Age. Valanginian to middle Aptian–early Albian (Valanginian to *Costata* Subzone of *Turbocapsula* Zone; zone after O'Dogherty, 1994) based on the presence of *Cryptamphorella clivosa* (Aliev) with *Praeconosphaera* (?) *sphaeroconus* (Rüst). Ranges after Aliev (1967), O'Dogherty (1994), Filippov & Kemkin (2005), Chiari, Cobianchi & Picotti (2007) and Bandini *et al.* (2011).

4.g. Section 8

TU10.47. Archaeodictyomitra excellens (Tan) (Fig. 5t), *Archaeodictyomitra lacrimula* (Foreman), *Archaeodictyomitra* sp. cf. *A. communis* (Squinabol), *Archaeodictyomitra* sp. cf. *A. ioniana* Danelian, *Archaeodictyomitra* sp. cf. *A. vulgaris* Pessagno, *Archaeodictyomitra* sp., *Archaeodictyomitra* (?) sp., *Cana septemporatus* (Parona) (Fig. 5u), *Halesium* sp. cf. *H. palmatum* Dumitrica (Fig. 5v), *Hiscocapsa* sp. cf. *H. grutterinki* (Tan), *Hiscocapsa* sp., *Holocryptocanium barbui* Dumitrica, *Holocryptocanium* sp. cf. *H. barbui* Dumitrica, *Pantanellium* sp., *Praeconosphaera* (?) sp. cf. *P.* (?) *sphaeroconus* (Rüst), *Praeconosphaera* (?) sp., *Pseudodictyomitra* sp. cf. *P.* sp. 5 in Dumitrica *et al.* (1997), *Pseudodictyomitra* sp., *Pseudodictyomitra* (?) sp., *Pseudoxitus* (?) sp., *Syringocapsa* (?) sp., *Thanarla* sp. cf. *T. brouweri* (Tan), *Thanarla* sp., *Thanarla* (?) sp., *Williriedellum* (?) sp., *Xitus* sp. cf. *X. normalis* (Wu & Li), *Xitus* sp., *Xitus* (?) sp.

Age. Late Valanginian–early Barremian (UAZ. 17–21; UAZones after Baumgartner *et al.* 1995*a*) based on the presence of *Cana septemporatus* (Parona). Ranges after Baumgartner *et al.* (1995*b*).

TU10.48. Age not determinable because of the very low preservation of radiolarians.

TU10.51. Acaeniotyle sp. cf. *A. umbilicata* (Rüst), *Archaeodictyomitra lacrimula* (Foreman) (Fig. 5w), *Archaeodictyomitra* sp. cf. *A. communis* (Squinabol), *Archaeodictyomitra* sp., *Archaeodictyomitra* (?) sp., *Crucella* (?) sp., *Praeconosphaera* (?) sp., *Pseudodictyomitra* (?) sp., *Pseudoeucyrtis* sp. cf. *P. hanni* (Tan) *sensu* O'Dogherty (1994) (Fig. 5x), *Spinosicapsa* (?) sp., *Thanarla* sp. cf. *T. pulchra* (Squinabol), *Thanarla* sp.

Age. Early–early late Berriasian to middle Aptian–early Albian (UAZ. 14 – *Costata* Subzone of *Turbocapsula* Zone; zone after O'Dogherty, 1994; UAZone after Baumgartner *et al.* 1995*a*) based on the presence of *Archaeodictyomitra lacrimula* (Foreman). Range after Baumgartner *et al.* (1995*b*) and O'Dogherty (1994).

TU10.M10. Archaeodictyomitra sp., *Archaeodictyomitra* (?) sp., *Kilinora* (?) sp., *Triversus* (?) sp.

Age. Age not determinable because of the low preservation of radiolarians.

5. Petrography and geochemistry of the basaltic rocks

5.a. Petrography

All the studied rocks are affected by low-temperature, ocean-floor alteration, which resulted in the replacement of primary minerals, though primary igneous textures are well preserved. Plagioclase is

usually replaced by albite or calcite and rarely by clay mineral assemblages. Clinopyroxene is normally pseudomorphosed either by chlorite or actinolitic amphibole. In samples TU10.22 and TU10.23 (Section 3) clinopyroxene is replaced by brown hornblende, though fresh clinopyroxene relics are locally observed. The groundmass secondary phases mainly consist of chlorite and clay minerals. Regardless of the secondary mineralogical transformation, the following petrographic description of the various rock types has been made on the basis of the primary igneous phases. Moreover, for a better understanding, it has been made according to the geochemical groups described below.

Group 1. Pillow and massive lavas have aphyric, micro-crystalline sub-ophitic textures in which only small laths of plagioclase can be recognized. Pillow breccias are generally monogenetic and show a coarse-grained, intergranular texture with euhedral plagioclase and interstitial clinopyroxene.

Group 2. Massive lavas show both aphyric and porphyritic (PI = ~40) textures. In both varieties, the groundmass texture is hyalopilitic. Phenocrysts are represented by large crystals of plagioclase.

Groups 3 and 4. Pillow and massive lavas most commonly display aphyric, ophitic or sub-ophitic textures with crystal sizes ranging from micro-crystalline to coarse grained. Nonetheless, a few samples display slightly porphyritic textures with plagioclase microphenocrysts. In addition, a hyalopilitic texture is locally observed. The groundmass mineral assemblage includes plagioclase, clinopyroxene and variable amounts of opaque phases. Pillow breccias are generally monogenetic and the individual fragments are texturally and compositionally similar to the pillow lavas. Most of these rocks are characterized by variable abundances of varioles filled by calcite. In all the studied rock groups, the crystallization order is: plagioclase + clinopyroxene ± Fe–Ti-oxides.

5.b. Analytical methods

Whole-rock major- and some trace-element analyses were obtained by X-ray fluorescence (XRF) on pressed-powder pellets, using an ARL Advant-XP automated X-ray spectrometer. The matrix correction methods proposed by Lachance & Trail (1966) were applied. Volatile contents were determined as loss on ignition (LOI) at 1000 °C. In addition, Rb, Sr, Nb, Hf, Ta, Th, U and the rare earth elements (REEs) were determined on 12 representative samples by inductively coupled plasma-mass spectrometry (ICP-MS) using a Thermo Series X-I spectrometer.

The CO_2 content was determined by the simple volumetric technique (Jackson, 1958) only on the samples affected by calcite veins and amygdales. This technique was calibrated using standard amounts of reagent grade $CaCO_3$. In addition, for the discussion of the geochemical characteristics and for a better comparison of chemical data, the major-element compositions of these samples were recalculated on a calcite-free basis. In detail, CaO content in secondary calcite has been calculated according to stoikiometric proportions with CO_2 contents, given that the secondary carbonates are exclusively composed of calcite. Major-element composition has then been recalculated to 100 wt % without considering LOI and CaO in calcite.

The accuracy of the data for XRF and ICP-MS analyses were evaluated using results for international standard rocks run as unknowns. The detection limits for XRF and ICP-MS analyses were evaluated using results from several runs of ~29 international standards. Accuracy and detection limits for the CO_2, analyses were determined using different amounts of reagent grade $CaCO_3$ run as unknowns. Results are given in the online Supplementary Material available at http://journals.cambridge.org/geo. All whole-rock analyses were performed at the Dipartimento di Science della Terra, Università di Ferrara. The results are shown in Table 1.

5.c. Geochemistry

The following geochemical description is made mainly using those major and trace elements that are virtually immobile during low-temperature alteration and metamorphism (e.g. Pearce & Norry, 1979). These elements include many incompatible elements, such as Ti, P, Zr, Y, Sc, Nb, Ta, Hf, Th, middle (M-) and heavy (H-) REEs, as well as some transition metals (e.g. Ni, Co, Cr, V). Light REEs (LREEs) may be affected by some mobilization during alteration. However, the good correlations between these elements and many immobile elements (not shown) indicate that LREEs have not been mobilized by the alteration. For example, the correlation coefficients (r^2) for the linear correlation Zr–La and Zr–Ce are 0.96 and 0.90, respectively. Rb, Ba, K and Sr are commonly mobilized during alteration. In fact, these elements plotted against Zr generally show low or very low r^2. However, the fairly good correlation with Zr and Rb in Group 4 samples ($r^2 = 0.91$), as well as Ba in Group 4 ($r^2 = 0.87$) and in Group 2 samples ($r^2 = 0.85$), suggests that these elements were only slightly mobilized during alteration in these rock types.

According to Bortolotti *et al.* (2013*a*), four groups of volcanic rocks can be recognized in the studied sections. Group 1 is represented by basalts cropping out in Sections 5 and 8. These rocks have a clear sub-alkaline nature with low Nb/Y ratios (Fig. 6) and show relatively high TiO_2, P_2O_5, Zr and Y contents. Ni is generally low, whereas Cr is relatively high, with the only exception of sample TU10.49b. V content is also generally high (Table 1). The values of these elements are similar to those of Group 2 basalts (see below). By contrast, Hf, Ta, Th and U contents are low. These rocks show a sharp increase in FO_t and Y and a sharp decrease in Mg no. and Ni with increasing Zr, as well as very low Th/Tb ratios (Fig. 7). Group 1 basalts are characterized by flat normalized incom-

Table 1. Representative major- and trace-element analyses of Middle Jurassic – Early Cretaceous volcanic rocks from the Ankara Mélange

Section	1			2				3		
Sample	TU10.6	TU10.9	TU10.10	TU10.14	TU10.15	TU10.16	TU10.17	TU10.19	TU10.22	TU10.23
Rock	bas	tra	bas	bas	bas	Fe-bas	Fe-bas	bas	bas	bas
Group	4	4	4	3	3	3	3	4	4	4
Type	alkaline OIB	alkaline OIB	alkaline OIB	trans P-MORB	trans P-MORB	trans P-MORB	trans P-MORB	alkaline OIB	alkaline OIB	alkaline OIB
Age	E Cr			M Jr	M Jr	M Jr	M Jr		L Jr	L Jr
Note	pillow	breccia	pillow	pillow	pillow	pillow	pillow	mlf	pillow	pillow
	(XRF)	*(XRF)*	*(XRF)*	*(XRF)*	*(XRF)*	*(XRF)*	*(XRF)*	*(XRF)*	*(XRF)*	*(XRF)*
SiO_2	41.40	56.12	39.61	44.12	40.20	42.40	44.87	44.36	46.03	44.81
TiO_2	1.91	2.35	1.96	2.28	1.65	3.27	2.55	2.97	2.32	2.21
Al_2O_3	11.76	15.96	11.81	14.48	11.92	13.81	13.82	13.41	17.06	16.49
Fe_2O_3	0.93	1.33	1.00	1.74	1.00	2.08	1.96	1.45	1.42	1.40
FeO	6.18	8.90	6.67	11.60	6.66	13.89	13.06	9.63	9.47	9.31
MnO	0.15	0.11	0.12	0.23	0.22	0.19	0.19	0.40	0.20	0.20
MgO	4.24	1.68	3.86	9.25	6.32	7.42	9.98	9.14	7.31	9.05
CaO	16.69	3.61	17.84	8.16	18.02	8.04	6.23	6.96	6.48	7.45
Na_2O	3.73	7.37	2.93	2.39	2.11	3.07	1.74	3.24	2.07	1.84
K_2O	1.72	0.65	2.06	0.82	1.89	0.69	1.26	1.13	3.54	2.95
P_2O_5	0.48	0.59	0.60	0.33	0.21	0.54	0.62	0.52	0.96	0.86
L.O.I.	10.94	1.16	11.56	4.65	9.89	4.65	3.73	6.94	3.15	3.50
Total	100.13	99.84	100.03	100.05	100.08	100.05	100.01	100.15	100.01	100.06
CO_2	6.23		6.13		7.05					
Mg no.	55.0	25.2	50.8	58.7	62.9	48.8	57.7	62.8	57.9	63.4
Zn	73	104	57	72	63	110	101	109	75	72
Cu	25	35	44	77	71	59	57	69	40	40
Sc	23	9	18	36	40	43	35	36	8	10
Ga	15	14	16	21	15	24	20	16	17	19
Ni	70	26	54	78	53	8	11	100	25	42
Co	27	16	23	37	33	37	30	36	23	25
Cr	227	56	115	135	81	26	21	271	16	29
V	204	180	206	334	275	403	329	474	188	210
Ba	289	186	340	246	717	199	177	193	1980	1380
Pb	4	7	5	7	4	7	6	16	8	7
Zr	217	320	225	165	128	239	196	265	330	287
	(ICP-MS)		*(ICP-MS)*	*(ICP-MS)*	*(ICP-MS)*			*(ICP-MS)*		*(ICP-MS)*
Rb	30.8	12.0	36.7	8.41	17.6	8.0	16.0	27.2	75.0	58.5
Sr	575	441	478	292	280	391	371	197	740	760
Y	28.5	40.0	29.3	22.0	27.6	58.0	48.0	29.0	39.0	36.1
La	40.3	64.0	39.0	20.7	24.6	50.0	45.0	49.7	65.0	58.9
Ce	70.3	192.0	70.9	43.0	46.7	129.0	82.0	85.3	160.0	109.0
Pr	8.01		8.14	4.91	5.35			9.25		11.3
Nd	27.2	45.0	28.1	18.1	19.1	33.0	30.0	30.4	60.0	39.7
Sm	5.84		6.07	4.63	4.54			6.11		9.08
Eu	1.77		1.84	1.53	1.53			1.69		2.77
Gd	4.50		4.69	4.60	4.45			4.62		7.11
Tb	0.702		0.722	0.718	0.657			0.697		1.03
Dy	3.71		3.76	4.28	3.82			3.67		5.33
Ho	0.704		0.711	0.896	0.793			0.707		0.992
Er	1.78		1.78	2.38	2.11			1.81		2.58
Tm	0.239		0.236	0.339	0.295			0.242		0.35
Yb	1.49		1.49	2.21	1.92			1.54		2.19
Lu	0.214		0.213	0.335	0.291			0.221		0.324
Nb	61.5	83.0	65.9	30.6	40.4	50.0	45.0	88.0	142.0	88.0
Hf	5.11	5.00	5.34	4.56	3.69	4.00	3.00	4.82	5.00	7.00
Ta	2.93		3.71	1.76	3.34			4.77		7.13
Th	5.09	9.00	5.49	2.77	3.48	7.00	5.00	7.49	9.00	11.6
U	1.48		1.34	0.793	1.04			1.75		2.99
$(La/Sm)_N$	4.46		4.15	2.88	3.49			5.25		4.19
$(Sm/Yb)_N$	4.36		4.52	2.33	2.63			4.40		4.62
$(La/Yb)_N$	19.43		18.75	6.72	9.17			23.13		19.33
Ti/V	69	79	71	43	44	51	48	40	76	65
Ce/Y	2.40	4.80	2.69	1.87	1.64	2.20	1.60	3.16	4.10	4.01
Nb/Yb	41.32		44.13	13.86	21.03			57.02		40.25
(Th/Ta)/(Th/Tb)	0.24		0.19	0.41	0.20			0.15		1.14

Table 1. Continued

Section	4		5			7	8		9	
Sample	TU10.32	TU10.33	TU10.34	TU10.39	TU10.40	TU10.46	TU10.49a	TU10.49b	TU10.52	TU10.53
Rock	bas	bas	bas	bas	bas	bas	bas	bas	bas	bas
Group	2	2	1	1	1	2	1	1	3	3
Type	sub-alk	sub-alk	sub-alk	sub-alk	sub-alk	sub-alk	sub-alk	sub-alk	trans	trans
E-MORB	E-MORB	G-MORB	G-MORB	G-MORB	E-MORB	G-MORB	G-MORB	P-MORB	P-MORB	
Age	E Cr	E Cr	L Jr	L Jr	L Jr	E Cr	E Cr	E Cr		
Note	mlf	mlf	mlf	breccia	mlf	mlf	pillow	pillow	mlf	mlf
(XRF)	*(XRF)*	*(XRF)*	*(XRF)*	*(XRF)*	*(XRF)*	*(XRF)*	*(XRF)*	*(XRF)*	*(XRF)*	
SiO_2	45.98	46.18	47.04	48.28	46.35	48.35	53.76	48.67	48.72	39.89
TiO_2	1.51	1.46	1.48	1.46	1.74	1.20	1.51	1.46	1.89	1.37
Al_2O_3	13.44	13.30	13.50	14.84	15.70	17.65	13.26	13.83	17.70	11.71
Fe_2O_3	1.44	1.26	1.28	1.42	1.59	0.77	1.28	1.65	1.42	1.05
FeO	9.61	8.43	8.51	9.49	10.60	5.14	8.52	11.01	9.49	6.97
MnO	0.29	0.27	0.26	0.19	0.11	0.11	0.13	0.16	0.05	0.17
MgO	5.69	5.14	5.24	5.48	2.40	4.69	5.80	7.48	3.77	4.26
CaO	14.15	15.60	15.85	9.28	12.16	9.55	8.03	6.18	4.16	21.76
Na_2O	2.82	3.21	3.27	3.39	3.77	5.71	3.88	2.49	2.04	1.88
K_2O	0.46	0.40	0.41	1.49	1.31	0.29	0.36	0.88	4.64	0.53
P_2O_5	0.14	0.13	0.14	0.17	0.28	0.12	0.17	0.11	0.32	0.14
L.O.I.	4.58	4.66	3.02	4.56	3.94	6.45	3.2	6.02	5.83	10.28
Total	100.11	100.06	100.00	100.05	99.95	100.03	99.89	99.94	100.04	100.01
CO_2	1.80	2.27	0.95		0.93					7.00
Mg#	51.4	52.1	52.3	50.7	28.8	61.9	54.8	54.8	41.4	52.2
Zn	84	87	87	115	124	63	79	97	115	63
Cu	77	94	92	62	27	95	55	12	35	27
Sc	42	39	44	55	48	26	19	40	28	32
Ga	16	14	16	18	17	14	21	18	16	19
Ni	139	139	139	106	69	40	32	15	140	213
Co	39	41	41	33	32	33	26	24	35	36
Cr	389	371	372	197	273	266	67	18	392	305
V	390	377	370	300	368	194	176	380	317	333
Ba	83	75	73	69	130	132	116	173	274	85
Pb	4	3	3	5	n.d.	3	5	6	6	6
Zr	74	73	73	97	98	75	84	88	135	84
	(ICP-MS)		*(ICP-MS)*	*(ICP-MS)*		*(ICP-MS)*		*(ICP-MS)*	*(ICP-MS)*	
Rb	6.35	5.00	25.2	28.4	17.0	3.15	2.00	14.8	68.8	2.00
Sr	130	136	129	385	201	429	120	129	160	96
Y	31.8	27.0	14.8	19.9	40.0	12.5	29.0	26.3	28.1	26.0
La	5.63	5.00	2.76	3.15	3.00	5.16	3.00	3.77	14.5	13.0
Ce	14.0	12.0	7.84	9.59	n.d.	11.8	9.0	10.1	26.2	31.0
Pr	2.18		1.32	1.59		1.63		1.67	3.38	
Nd	10.1	9.00	6.49	7.88	13.0	7.59	10.0	8.91	14.0	10.0
Sm	3.24		2.16	2.61		2.20		2.99	3.59	
Eu	1.13		0.778	0.907		0.811		1.10	1.06	
Gd	4.21		2.68	3.21		2.72		3.99	4.13	
Tb	0.752		0.470	0.560		0.463		0.714	0.698	
Dy	5.04		3.03	3.63		2.95		4.70	4.42	
Ho	1.15		0.638	0.791		0.626		1.01	0.869	
Er	3.23		1.70	2.15		1.75		2.78	2.43	
Tm	0.478		0.247	0.320		0.258		0.401	0.354	
Yb	3.18		1.52	2.03		1.69		2.54	2.24	
Lu	0.492		0.224	0.304		0.258		0.362	0.322	
Nb	7.81	9.00	2.88	3.36	5.00	5.25	4.00	2.74	25.7	19.0
Hf	2.78	3.00	1.61	2.24	n.d.	2.45	3.00	1.81	3.51	n.d.
Ta	0.404		0.161	0.188		0.277		0.159	1.480	
Th	0.619	n.d.	0.112	0.211	1.00	0.342	n.d.	0.195	2.51	3.00
U	0.151		0.071	0.008		0.102		0.052	0.573	
$(La/Sm)_N$	1.12		0.82	0.78		1.51		0.81	2.61	
$(Sm/Yb)_N$	1.13		1.58	1.43		1.45		1.31	1.78	
$(La/Yb)_N$	1.27		1.30	1.12		2.19		1.06	4.65	
Ti/V	25	25	25	31	30	40	53	25	38	31
Nb/Y	0.27	0.30	0.14	0.12	0.20	0.25	0.20	0.09	0.86	0.70
Nb/Yb	2.46		1.90	1.66		3.12		1.08	11.46	
(Th/Ta)/(Th/Tb)	1.86		2.91	2.98		1.67		4.50	0.88	

Abbreviations: bas – basalt; tra – trachyte; Fe-bas – ferrobasalt; trans – transitional-type; sub-alk – sub-alkaline-type; OIB – ocean-island basalt; P-MORB – plume-type mid-ocean ridge basalt; E-MORB – enriched-type mid-ocean ridge basalt; G-MORB – garnet-influenced mid-ocean ridge basalt; E – Early; M – Middle; L – Late; Jr – Jurassic; Cr – Cretaceous; mlf – massive lava flow; n.d. – not detected. Mg no. $= 100 \times Mg/(Mg + Fe^{2+})$. $Fe_2O_3 = 0.15 \times FeO$. Normalizing values for REE ratios are from Sun & McDonough (1989).

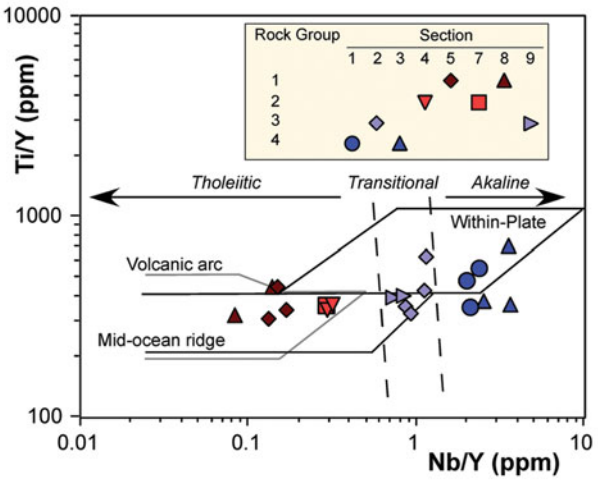

Figure 6. (Colour online) Ti/Y v. Nb/Y discrimination diagram (Pearce, 1982) for Middle Jurassic – Early Cretaceous volcanic rocks from the Ankara Mélange. Modified from Bortolotti *et al.* (2013*a*).

patible element patterns (Fig. 8a). The REE abundance (Fig. 8b) varies from ~10 to ~20 times that of chondrite and displays LREE/MREE smoothly depleted patterns with $(La/Sm)_N$ ratios ranging from 0.78 to 0.82. The overall geochemical features of these rocks, as well as both the incompatible elements and REE patterns, resemble those of typical N-MORB (normal mid-ocean ridge basalt) (Sun & McDonough, 1989). Nonetheless, HREEs are slightly depleted with respect to both LREEs and MREEs (Fig. 8b) with $(La/Yb)_N$ ratios = 1.06–1.30 and $(Sm/Yb)_N$ ratios = 1.31–1.58. In particular, the $(Sm/Yb)_N$ ratios are higher than that of typical N-MORB (Sm_N/Yb_N = 0.96, Sun & McDonough, 1989). These values are comparable to those of garnet-influenced MORBs (G-MORB) from the External Ligurides of the Northern Apennines (Sm_N/Yb_N = 1.25–1.50, Montanini, Tribuzio & Vernia, 2008), Corsica (Sm_N/Yb_N = 1.30–1.81, Saccani *et al.* 2008*b*) and Elba Island (Sm_N/Yb_N = 1.49–2.10, Saccani & Principi, 2016), as well as to those of the Palaeozoic Misho mafic complex in north Iran (Saccani *et al.* 2013*a*) and the Mesozoic Kermanshah ophiolites in south Iran (Saccani *et al.* 2013*b*). The G-MORB affinity of Group 1 rocks is also suggested by Th–Nb co-variation and by their $(Ce/Yb)_N$ and $(Dy/Yb)_N$ ratios (Fig. 9), although in the most common tectonic discrimination diagrams these basalts plot in the field for N-MORBs (e.g. Fig. 10).

Group 2 is represented by basalts cropping out in Sections 4 and 7. These rocks have a sub-alkaline nature with low Nb/Y ratios ranging from 0.27 to 0.40 (Fig. 6) and show relatively high TiO_2, P_2O_5, Zr and Y contents (Table 1). Ni, though variable, is generally low, whereas Cr and V are rather high. As exemplified in the variation diagrams in Figure 7, these rocks have major-element contents and compositions of many trace elements largely overlapping those of Group 1 basalts. Nonetheless, as a distinctive feature, Group 2 basalts are characterized by large ion lithophile element (LILE)/high-field-strength element (HFSE) smoothly enriched patterns (Figs 8c). Likewise, REE patterns show a slight enrichment in LREEs compared to HREEs (Fig. 8d), with $(La/Sm)_N$ and $(La/Yb)_N$ ratios ranging from 1.12 to 1.51 and from 1.27 to 2.19, respectively. These patterns are similar to that of the typical enriched-type MORB (E-MORB) of Sun & McDonough (1989). The Th–Nb values are also similar to those of the typical E-MORB (Fig. 9a). In the most common tectonic discrimination diagrams these basalts plot across the boundary between the fields for N-MORB and E-MORB (e.g. Fig. 10).

Group 3 is represented by pillow basalts and ferrobasalts from Section 2, as well as by massive lava basalts from Section 9. These rocks have a transitional nature, as testified to by their high Nb/Y ratios (Fig. 6). Basalt TU10.15 (Section 2) displays a rather primitive composition with relatively high Mg no. and low TiO_2 and P_2O_5 contents (Table 1). In contrast, ferrobasalts from Section 2 and basalts from Section 9 have rather evolved compositions with relatively low Mg no. and very high TiO_2 and P_2O_5 contents (Table 1). Accordingly, Ni and Cr contents are generally high in basalts, whereas they are relatively low in the differentiated rocks. Except for Mg no., the variation of many elements with respect to Zr display roughly common evolutionary trends towards high contents of the incompatible elements and FeO_t and low contents of the compatible elements for all Group 3 samples (Fig. 7). In contrast, Mg no. for samples from Sections 2 and 9 show distinct evolutionary trends with respect to Zr. All these trends are compatible with a magmatic evolution by fractional crystallization. The Th/Tb ratios of these rocks are significantly higher than those of Groups 1 and 2 rocks and significantly lower than those of Group 4 rocks (Fig. 7). Group 3 rocks show high abundance in low-field-strength elements (LFSEs) with respect to N-MORB and display regularly decreasing N-MORB normalized patterns from Rb to Y (Fig. 8e). The REE abundance (Fig. 8f) varies from ~30 to ~100 and from ~10 to ~12 times that of chondrite for LREEs and HREEs, respectively. These rocks displays LREE/MREE and LREE/HREE enriched patterns, with $(La/Sm)_N$ ratios = 2.61–4.15 and $(La/Yb)_N$ ratios = 4.65–9.17. These incompatible elements and REE patterns are comparable to those of P-MORB (plume-type MORB). This conclusion is also supported by the co-variation of the Th and Nb concentrations (Fig. 9a). In the most common tectonic discrimination diagrams (e.g. Fig. 10) these rocks generally plot in the fields for E-MORBs and alkaline ocean-island basalts (OIB).

Group 4 is represented mainly by alkaline basalts and subordinate trachytes from Sections 1 and 3. These rocks have a clear alkaline nature, as testified to by their very high Nb/Y ratios (Fig. 6). Alkaline basalts from Section 3 mainly display relatively primitive compositions, whereas alkaline basalts from Section 1 represent rather evolved compositions. Generally, all

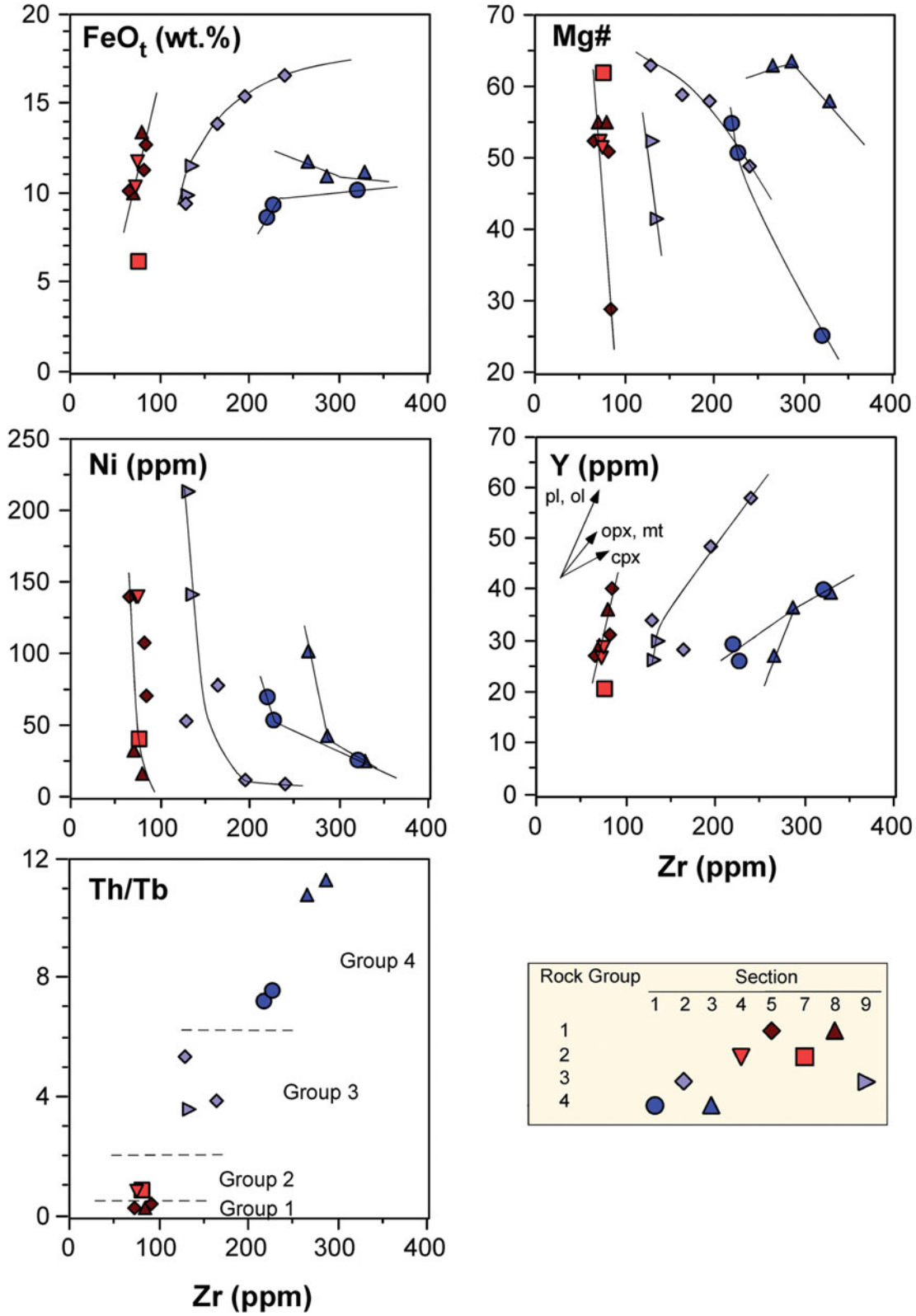

Figure 7. (Colour online) Variation diagrams for some representative major and trace elements versus Zr for Middle Jurassic – Early Cretaceous volcanic rocks from the Ankara Mélange. Major elements are recalculated on a volatile-free and calcite-free basis. Abbreviations: pl – plagioclase; ol – olivine; cpx – clinopyroxene; opx – orthopyroxene; mt – magnetite. Mg no. $= 100 \times Mg/(Mg + Fe^{2+})$. Lines represent the inferred fractionation trends for the different rock groups.

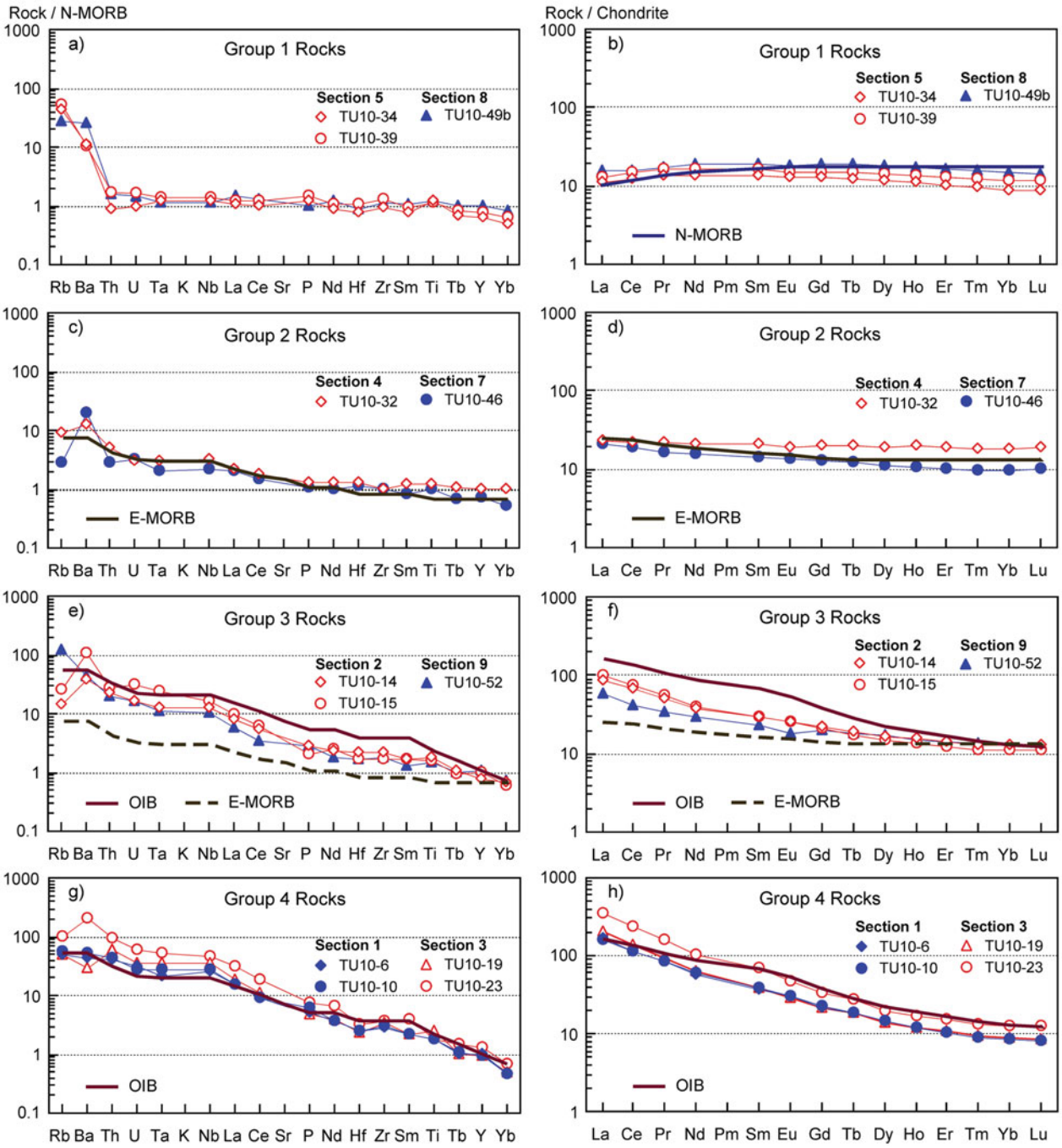

Figure 8. (Colour online) (a, c, e, g) N-MORB normalized incompatible element patterns and (b, d, f, h) chondrite-normalized REE patterns for Middle Jurassic – Early Cretaceous volcanic rocks from the Ankara Mélange. Normalizing values and the compositions of normal mid-ocean ridge basalt (N-MORB), enriched mid-ocean ridge basalt (E-MORB) and ocean-island basalt (OIB) are from Sun & McDonough (1989).

samples have high contents of TiO_2, P_2O_5, Zr, Nb, Hf and Th and low contents of compatible elements (Table 1; Fig. 7). In the variation diagrams in Figure 7, rocks from the different sections show different evolutionary trends, most likely reflecting the distinct evolutions of magmas of different initial compositions. This is particularly evident in the FeO_t, Mg no., Ni and Y v. Zr diagrams. Nonetheless, the well-defined trends observed for samples from each single section suggest that each section consists of rocks belonging to a comagmatic suite. Group 4 rocks show high abundance in LFSEs with respect to N-MORB and display regularly decreasing N-MORB normalized patterns from Rb to Y (Fig. 8g). The REE abundance (Fig. 8h) varies from ~60 to ~400 and from ~9 to ~10 times that of chondrite for LREEs and HREEs, respectively. These rocks displays LREE/MREE and LREE/HREE strongly enriched patterns, with $(La/Sm)_N$ ratios = 4.15–5.25 and $(La/Yb)_N$ ratios = 18.75–23.13. Group 4 rocks can readily be distinguished from Group

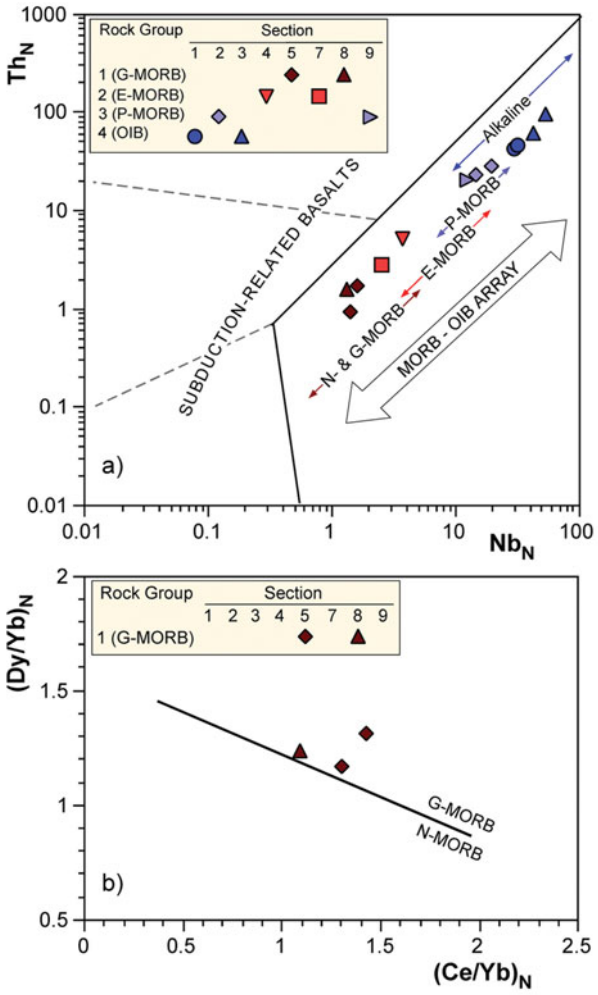

Figure 9. (Colour online) (a) Th_N v. Nb_N and (b) $(Dy/Yb)_N$ v. $(Ce/Yb)_N$ discrimination diagrams for Middle Jurassic – Early Cretaceous volcanic rocks from the Ankara Mélange. Modified after Saccani (2015). N-MORB and chondrite normalization values for panels (a) and (b), respectively, are from Sun & McDonough (1989).

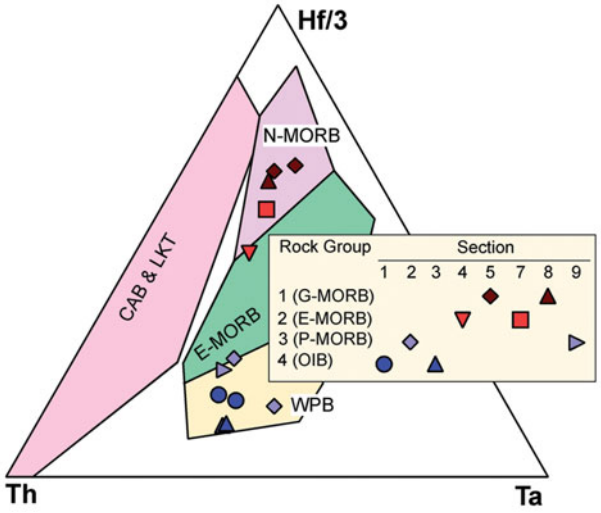

Figure 10. (Colour online) Th–Ta–Hf/3 (Wood, 1980) discrimination diagrams for Middle Jurassic – Early Cretaceous volcanic rocks from the Ankara Mélange.

3 rocks, as they show higher Zr, incompatible element and LREE concentrations, as well as Th/Tb ratios at comparable Mg no. (Figs 7, 8g, h). The overall geochemistry of these basalts resembles that of alkaline basalts generated at within-plate ocean-island settings (OIB), as also exemplified by the generally high Ti/V ratios (Table 1). This conclusion is also supported by the co-variation of the Th and Nb values (Fig. 9), as well as by the most common tectonic discrimination diagrams (e.g. Fig. 10).

6. Discussion

6.a. Mantle melting processes and magma generation

One of the main goals of this study is to assess the nature and tectonic significance of the magmatic events that occurred in the Turkish sector of the Neotethys during the Middle Jurassic – Early Cretaceous time span. According to many authors (e.g. Pearce, 1982), the compositional differences between magma types are related to different source characteristics that are associated, in turn, with distinct tectonomagmatic settings of formation. We will therefore focus our petrogenetic discussion on the identification of the possible mantle sources and related tectonic setting of formation of the four distinct lava groups identified in the previous section, which are: (1) G-MORBs (Group 1); (2) E-MORBs (Group 2); (2) P-MORBs (Group 3); (4) OIB-type alkaline volcanic rocks (Group 4). Unfortunately, the chemical variation due to fractional crystallization cannot be defined in detail, as the mélange nature of the sampled rocks prevents us from establishing definite genetic relationships between rocks within each single chemical group. Nonetheless, some trace-element ratios (e.g. Zr/Nb, Ce/Y, Th/Ta, Th/Tb) are little affected by fractional crystallization of predominantly olivine + clinopyroxene + plagioclase. Therefore, even in the presence of significant amounts of fractionation, they are believed to represent the elemental ratios in the source (e.g. Allègre & Minster, 1978; Beker *et al.* 1997). Ratios of incompatible elements (Ce/Y, Nb/Yb), ratios of hygromagmatophile element ratios ((Th/Ta)/(Th/Tb)) (Table 1), as well as distinct normalized multi-element and REE patterns (Fig. 8) suggest that the different magmatic rocks from the Ankara Mélange units have been most likely originated from chemically distinct mantle sources. In order to constrain the possible mantle sources of the different rock series of the Ankara Mélange, non-modal, batch partial melting models are presented in Figure 11. A rigorous quantification of the melting processes is not possible as the composition of the mantle sources are difficult to constrain. However, a semi-quantitative modelling of the REEs can place some solid constraints. The melt modelling uses plots of LREE/HREE (i.e. La/Yb) v. MREE/HREE (i.e. Dy/Yb) ratios, which are particularly useful for distinguishing between melting in the

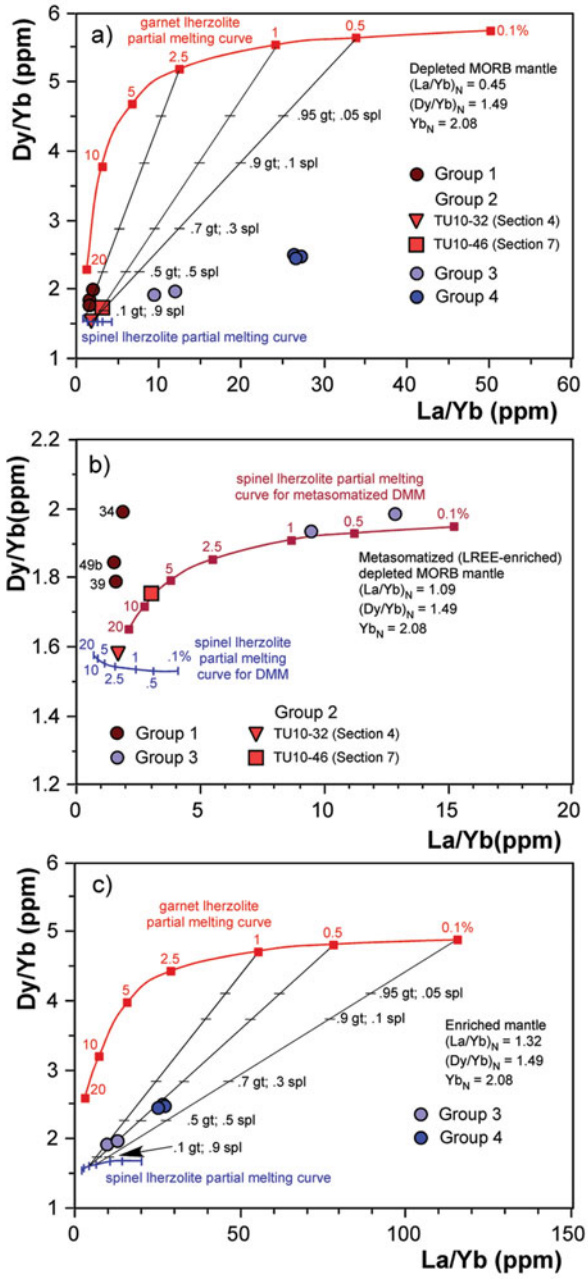

Figure 11. (Colour online) Melt curve models based on Dy/Yb v. La/Yb. Melt curves are calculated using non-modal, batch melts of garnet and spinel lherzolites. (a) Melt curves for DMM mantle (Workman & Hart, 2005); (b) melt curves for a theoretical DMM mantle (Workman & Hart, 2005) enriched in LREEs by OIB-type components; (c) melt curves for a theoretical enriched (OIB-type) mantle. Garnet lherzolite mode is: 0.598 ol, 0.211 opx; 0.076 cpx, 0.115 gt that melts in the proportions 0.05 ol, 0.20 opx, 0.30 cpx, 0.45 gt. Spinel lherzolite mode is: 0.578 ol, 0.270 opx, 0.119 cpx, 0.033 spl that melts in the proportions 0.10 ol, 0.27 opx, 0.50 cpx, 0.13 spl. Mantle mode and melting proportions are from Thirlwall, Upton & Jenkins (1994). Arrays representing the mixing between various proportions of melt fractions from the garnet-facies mantle and melt fractions from the spinel-facies mantle are also shown. Distribution coefficients are from Irving & Frey (1984) with the exception of those for spinel, which are from McKenzie & O'Nions (1991). Normalizing values are from Sun & McDonough (1989).

spinel and garnet stability fields (Thirlwall, Upton & Jenkins, 1994). Partial melting of a mantle source in the spinel-facies produces little change in Dy/Yb ratios in melts with respect to melt fraction. In contrast, mantle partial melting in the garnet-facies produces large changes in Dy/Yb ratios with melt fraction. In both cases, La/Yb ratios are particularly responsive to melt fraction change (Fig. 11). Another important feature of these plots is that mixing between different melt fractions will generate linear mixing arrays (e.g. Beker *et al.* 1997).

Group 1 basalts. As observed in the previous section, the Group 1 rocks (G-MORBs) show unusually high MREE/HREE ratios (Dy_N/Yb_N = 1.20–1.34) compared to the typical N-MORB (Dy_N/Yb_N = 1, Sun & McDonough, 1989). REE modelling for Group 1 basalts (Fig. 11a) shows that these rocks cannot have been simply derived from partial melting of a typical depleted MORB mantle (DMM) source (Workman & Hart, 2005) in the spinel-facies. Rather, their significant HREE/MREE fractionation can be interpreted as a garnet signature, which can be related either to a deep initiation of melting in the garnet peridotite stability field, or to the melting of a heterogeneous mantle source characterized by garnet-bearing mafic/ultramafic layers (e.g. Montanini, Tribuzio & Vernia, 2008; Saccani *et al.* 2008*b*; Saccani, 2015). However, melting of a DMM source bearing garnet mafic/ultramafic layers would generate primary melts characterized by high MREE/HREE ratios coupled with low (<0.8) LREE/HREE ratios (not shown). By consequence, the high (1.06–1.30) LREE/HREE ratios observed in the Group 1 basalts are inconsistent with this hypothesis. Therefore, in Figure 11a the partial melting model of a DMM source that starts in the garnet-facies and continues to larger degrees in the spinel-facies (with various combinations of melting fractions in the garnet- and spinel-facies) is shown. It can be observed that the REE composition of the Group 1 basalts is compatible with the calculated compositions for 2.5 % melting in the garnet-facies and 10 % melting in the spinel-facies, assuming mixing of ~70–80 % of melt derived from spinel-facies mantle with ~30–20 % melt from garnet-facies mantle.

Group 2 basalts. Group 2 basalts (E-MORBs) show variable LREE/HREE enrichments (Fig. 8d), which can be considered a result of variable mixing between depleted and enriched asthenospheric sources or, alternatively, from lower degrees of partial melting of a DMM source, compared to N-MORBs. In fact, basalt TU10.32 is generally compatible with a low degree (~2.5 %) of partial melting of a DMM source in the spinel-facies (Fig. 11b). However, basalt TU10.46 shows HREE values lower than those of the N-MORBs of Group 1, which cannot be generated by lower degrees of partial melting of a common mantle source (Fig. 8b, d). In addition, lower degrees of partial melting of a DMM source in the spinel-facies cannot generate the $(La/Yb)_N$ and $(Dy/Yb)_N$ ratios of this

sample. The most appropriate solution for the genesis of this E-MORB sample is not straightforward. The LREE/HREE and MREE/HREE ratios are compatible with mixing of melt derived from a very low degree (~1 %) of partial melting of a DMM source in the garnet-facies with melt derived from a much larger degree (~10 %) of partial melting in the spinel-facies mantle (Fig. 11a). The REE composition of these basalts is compatible with mixing of <10 % of melts generated in the garnet-facies with > 90 % of melts generated in the spinel-facies. Nonetheless, a possible alternative solution is to invoke a more enriched source than DMM. Figure 11b shows that the melting curve of a hypothetical DMM source slightly enriched in LREEs with $(La/Yb)_N = 1.09$ and $(Dy/Yb)_N = 1.49$, and has a Yb concentration equal to that of DMM ($Yb_N = 2.08$). The model shows that the REE composition of E-MORB TU10.46 is compatible with the calculated composition for ~8 % partial melting of this theoretical source in the spinel-facies.

Group 3 and Group 4 rocks. The high LREE/HREE ratios displayed by the transitional basalts of Group 3 rocks (P-MORBs) and by the alkaline basalts of Group 4 (Fig. 8f, h) suggest an involvement of a garnet peridotite source. Moreover, the high La/Yb ratio observed in these basalts implies a source more enriched in LREEs than DMM. In fact, variable degrees of partial melting of a DMM source in the spinel-facies cannot generate the observed La/Yb ratios, and variable degrees of partial melting of a DMM source in the garnet-facies cannot generate the observed La/Yb and Dy/Yb ratios (Fig. 11a). Therefore, the most appropriate solution is to invoke a more enriched source than DMM, although it is impossible to assess the exact composition of this source. The model in Figure 11c illustrates melting curves for a hypothetical LREE-enriched source (Beker *et al.* 1997) with $(La/Yb)_N = 1.32$ and $(Dy/Yb)_N = 1.49$, and has a Yb concentration equal to that of DMM ($Yb_N = 2.08$). Higher Yb concentrations (e.g. PM values) in the source would generate concentrations of HREEs in the melts that are too high compared with the Group 3 and Group 4 volcanic rocks.

The co-variation in La/Yb–Dy/Yb systematics of Group 3 and Group 4 samples (Fig. 11c) cannot, however, be explained by variable degrees of partial melting of this enriched source in either the spinel- or garnet-facies. Melting in the garnet-facies produces melts with much higher Dy/Yb ratios than those of both Group 3 and Group 4 samples at reasonable degrees of melting (i.e. <20 %). Alternatively, the mantle source would require an unusually low Dy/Yb ratio if the samples were to be simply the product of garnet-facies mantle melting. By contrast, melting in the spinel-facies produces melts with both La/Yb and Dy/Yb ratios lower than those of both Group 3 and Group 4 samples. Therefore, the simplest model to account for the REE systematics of these rocks involves mixing of small melt fractions from garnet-facies enriched mantle with relatively larger melt fractions from spinel-facies (Fig. 11c). This figure shows that the La/Yb–Dy/Yb systematics of Group 3 basalts can be explained by mixing of small-degree melts (~0.5–1 %) and larger degree melts (~5 %) from garnet- and spinel-facies mantle, respectively. Likewise, the observed REE data for Group 4 basalts can be accounted for by mixing of melts from ~0.5 % and ~5 % partial melting from garnet- and spinel-facies mantle, respectively. Alternatively, the La/Yb–Dy/Yb systematics of Group 4 basalts can be explained by a comparatively higher degree of melting (~1 %) in the garnet-facies mantle and comparatively lower degree of melting (~2.5 %) in the spinel-facies mantle. In any case, the different La/Yb–Dy/Yb ratios shown by Group 3 and Group 4 basalts can be accounted for by mixing of different proportions of melts generated in the garnet- and spinel-facies mantle. In detail, Group 4 basalts may have resulted from the mixing of ~60 % of melt derived from spinel-facies mantle with ~40 % melt from garnet-facies mantle, whereas Group 3 basalts may have resulted from the mixing of ~90 % of melt derived from spinel-facies mantle with ~10 % melt from garnet-facies mantle (Fig. 11c).

Figure 11b shows that the La/Yb and Dy/Yb ratios of Group 3 basalts can also be compatible with a very low degree (<0.8 %) of partial melting in the spinel-facies of the slightly metasomatized mantle source hypothesized for the genesis of Group 2 rocks. Such a very low degree of partial melting is, however, unreasonable. In fact, experimental studies on melt mobility in peridotites showed that very small melt fractions are not readily mobile and therefore they remain within the host peridotite rather than migrating to form volcanic rock melt (see Warren, 2016 for a more detailed discussion). Finally, it should be noted that variations in the degree of partial melting in the spinel field are difficult to constrain owing to the small range in La/Yb ratios generated by spinel-facies melting. Some scatter in the La/Yb–Dy/Yb systematics (Fig. 11c) might be accounted for by small fluctuations in the degree of melting of garnet-facies mantle. In any case, from a semi-quantitative point of view, melt fractions in the garnet field are restricted to <1 % whereas those in the spinel field are probably several per cent (~5 %).

The possible influence of crustal contamination can be excluded as the Th–Nb compositions of all rock types plot within the MORB–OIB array (Fig. 9). Other geochemical indicators further support this conclusion. For example, high Th/Ta and low Nb/U ratios are effective indicators of crustal contamination. All groups of Middle Jurassic – Early Cretaceous basalts from the Ankara Mélange show very low Th/Ta ratios (<1.74), as well as Nb/U ratios averaging 44 in N-MORBs, 50 in E-MORBs, 40 in P-MORBs and 43 in OIBs. These Nb/U ratios are comparable to those of the typical N-MORB (49.6), E-MORB (46.1) and OIB (47.1) of Sun & McDonough (1989).

Bortolotti *et al.* (2013*a*) have noted that the association of depleted basalts (N-MORBs), moderately

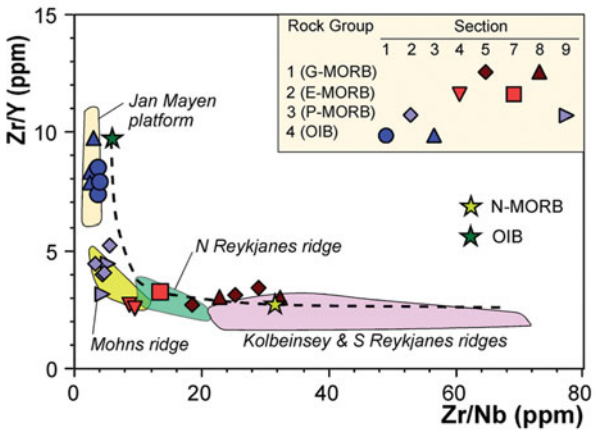

Figure 12. (Colour online) Zr/Y v. Zr/Nb diagram for volcanic rocks from the Middle Jurassic – Early Cretaceous volcanic rocks from the Izmir–Ankara Mélange (modified from Bortolotti *et al.* 2013*a*). The compositions of modern normal mid-ocean ridge basalt (N-MORB) and ocean-island basalt (OIB) are from Sun & McDonough (1989). The compositional variation for ocean-floor basalts erupted in the North Atlantic Ocean is shown for comparison (data from Hanan *et al.* 2000). The dashed line represents the mixing curve calculated using the OIB and N-MORB end-members.

enriched basalts (E-MORBs) and variably enriched rocks (P-MORBs and OIBs) occurring in the Ankara Mélange is also observed in many peri-Mediterranean ophiolitic complexes (e.g. Saccani & Photiades, 2005; Saccani *et al.* 2011 and references therein), as well as from several Middle East ophiolites (Allahyari *et al.* 2010; Saccani *et al.* 2010, 2013*a*,*b*), where it is interpreted as the result of partial melting of a MORB-type asthenospheric source enriched in HFSEs and LREEs by an OIB-type chemical component (plume-type component). Bortolotti *et al.* (2013*a*) have used the co-variation of Zr/Y and Zr/Nb to qualitatively depict the influence of a plume-type component on MORB compositions in the Middle Jurassic – Early Cretaceous basalts from the Ankara Mélange (Fig. 12). From Figure 12 it is evident that the data conform extremely well to the mixing curve calculated using the OIB and N-MORB end-members. Such mixing relationships are consistent with either magma mixing or source region mixing (or eventually, a combination of these).

6.b. Tectonomagmatic significance

The melting models carried out for the different groups of volcanic rocks, which are presented in the previous section, allow the following conclusions to be drawn: (1) the geochemically distinct groups of Middle Jurassic – Early Cretaceous volcanic rocks in the Ankara Mélange are related to different mantle source compositions and partial melting degrees; (2) regardless of their geochemical affinities, all the studied volcanic rocks were generated by partial melting starting in the garnet-facies mantle and continuing to larger degrees in the spinel-facies mantle. Perhaps, Group 2 basalts from Section 7 may represent the only exception to this conclusion. In fact, their chemistry is compatible either with partial melting starting in the garnet-facies mantle and continuing to larger degrees in the spinel-facies mantle, or partial melting in the spinel-facies from a slightly enriched source. As shown before, the formation of enriched alkaline and P-MORB-type rocks implies the occurrence of mantle sources strongly metasomatized by OIB-type components. Two alternative hypotheses can account for such OIB-type metasomatism of depleted mantle sources: (1) the existence of plume activity in the region during Middle Jurassic – Early Cretaceous times and (2) the existence of deep mantle heterogeneously modified by previous mantle plume activity that occurred in the same area in association with the opening of the Neotethys. However, the extant geological evidence suggests that the first hypothesis can be disregarded. In fact, the lack of magmatic evolution from more depleted to more enriched rocks that is commonly observed in plume-related magmatism, the absence of basaltic plateaus and a relatively small volume of plume-related volcanic rocks collectively argue against the existence of a well-established, long-lasting mantle plume in the region. Therefore, we favour the hypothesis that the different Middle Jurassic – Early Cretaceous volcanic rock types from the Ankara Mélange were formed from partial melting of a strongly heterogeneous mantle, with OIB-type components inherited from a previous mantle plume activity associated with the opening of the Neotethys. In fact, the Anisian alkaline volcanic rocks intruding the Kütahya–Bolkardag have been interpreted as the early products of the rifting of the Neotethys Ocean with the involvement of a plume (Göncüoglu, Turhan & Tekin, 2003; Göncüoglu, 2010; Akal *et al.* 2012). Recent studies on modern oceanic basins further support our favoured hypothesis. In fact, these studies have demonstrated that the upper mantle is much more heterogeneous than previously thought (e.g. Brunelli *et al.* 2006; Warren, 2016). The mantle heterogeneities can be either the result of earlier tectonic events or ancient episodes of melting, melt extraction and melt entrapment, and they can occur at a local or at a regional scale (e.g. Liu *et al.* 2008; Warren *et al.* 2009).

A possible tectonomagmatic model that can explain the formation of the different volcanic rocks from the Ankara Mélange during Middle Jurassic – Early Cretaceous times is shown in Figure 13. In this model, the OIB-type metasomatized portions are likely to be prominent in the asthenospheric mantle. The uprising asthenospheric mantle underwent polybaric partial melting, which started in the garnet-facies and continued in the spinel-facies. The strongly enriched alkaline and P-MORB rocks were generated from various, but limited degrees of polybaric partial melting of OIB-type metasomatized portions. G-MORB and E-MORB were generated from various degrees of polybaric partial melting of depleted asthenosphere portions. Alternatively, E-MORB (particularly, that of Section 7) may have been generated from partial

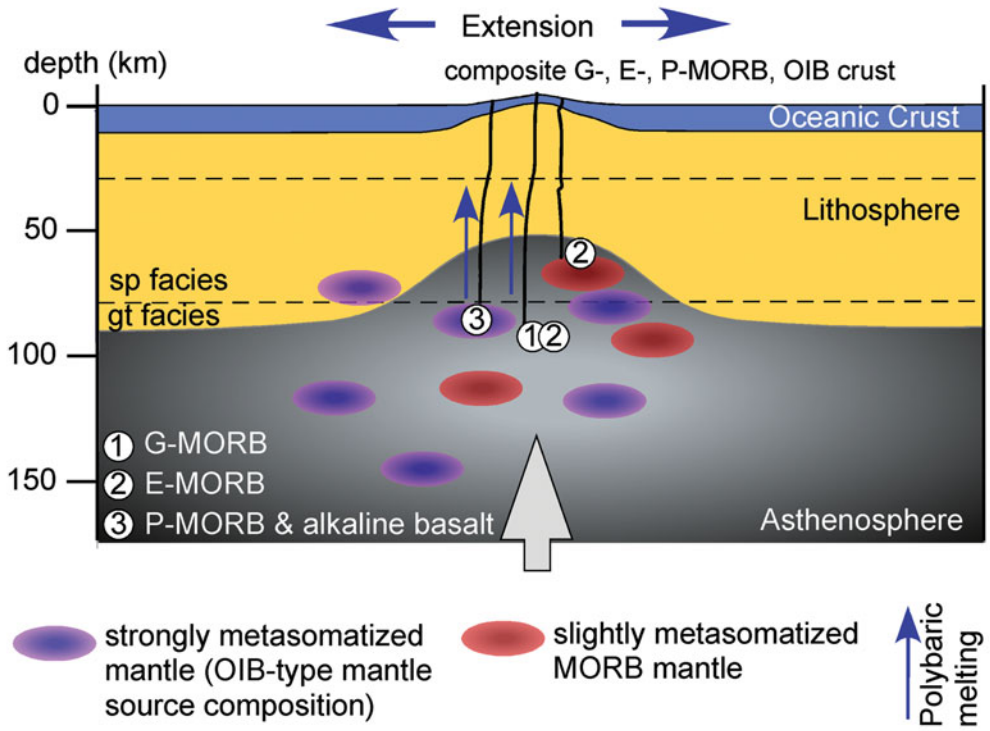

Figure 13. (Colour online) Two-dimensional cartoon showing the tectonomagmatic mechanisms responsible for the formation of garnet-influenced (G-), enriched (E-) and plume-type (P-) mid-ocean ridge basalts (MORB), as well as alkaline ocean-island-type (OIB) basalts from the Ankara Mélange during Late Jurassic – Early Cretaceous times. Other abbreviations: sp – spinel; gt – garnet.

melting of a slightly enriched mantle source in the spinel stability field. The tectonomagmatic model presented in Figure 13 implies that the different rocks were formed by partial melting of chemically different portions of the sub-oceanic mantle in different times. In consequence, this model does not necessarily imply the existence of a genetic relationship between different rock groups or within a single rock group.

6.c. Geodynamic implications

The ages obtained for the studied radiolarian assemblages coupled with the geochemistry of the associated basalts indicate that a composite oceanic crust including G-MORB, E-MORB, P-MORB and alkaline basalts was forming during Middle Jurassic – Early Cretaceous times. These ages are in agreement with the radiolarians (Bragin & Tekin, 1996; Tekin, 1999; S. Celik, unpub. M.Sc. thesis, Hacettepe Univ., 2010; T. Üner, unpub. Ph.D. thesis, Hacettepe Univ., 2010; Tekin, Göncüoglu & Uzuncimen, 2012; Göncüoglu *et al.* 2015) and foraminifera (Boccaletti, Bortolotti & Sagri, 1966; Bortolotti & Sagri, 1968; Yaliniz, Göncüoglu & Özkan-Altiner, 2000; Rojay, Yaliniz & Altiner, 2001) data obtained from different parts of the IAESB. The age ranges from the published biostratigraphical data indicate gaps in Early Jurassic and late Early Cretaceous times (see Göncüoglu, Sayit & Tekin, 2010). Moreover, Middle Jurassic findings were restricted to a limited number of samples. Our new findings partially fill the gap during the late Early Cretaceous period (see Göncüoglu, Sayit & Tekin, 2010). In fact, the radiolarian cherts associated with the G-MORB of Section 8 indicated a late Valanginian – early Barremian age.

The Middle Jurassic – Early Cretaceous rock assemblage found in the mélange complexes of the IAESB, as well as the tectonomagmatic model presented in the previous section can be framed within the geodynamic model presented by Göncüoglu (2010) (Fig. 14). According to this model, the rifting of the Neotethys Ocean started in Late Triassic time with the involvement of a mantle plume (Fig. 14a). Anisian and Norian volcanic rocks showing alkaline affinity were erupted at this stage (Göncüoglu, Turhan & Tekin, 2003; Göncüoglu 2010; Akal *et al.* 2012; Bortolotti *et al.* 2013*a*). The Early Jurassic history of this oceanic basin cannot be straightforwardly constrained owing to the lack of data. In fact, Early Jurassic (Hettanginian–Sinemurian) radiolarian chert blocks were found as single blocks in the Ankara Mélange, but they are not associated with volcanic rocks (S. Celik, unpub. M.Sc. thesis, Hacettepe Univ., 2010; Göncüoglu *et al.* 2015). Nonetheless, it is reasonable to postulate that during this time the Neotethys Ocean experienced an oceanic spreading phase. During the Middle Jurassic – Early Cretaceous time span the formation of a composite oceanic crust including G-MORB, E-MORB, P-MORB and alkaline basalts suggests that the volcanic rocks of the IAESB formed at a mid-ocean

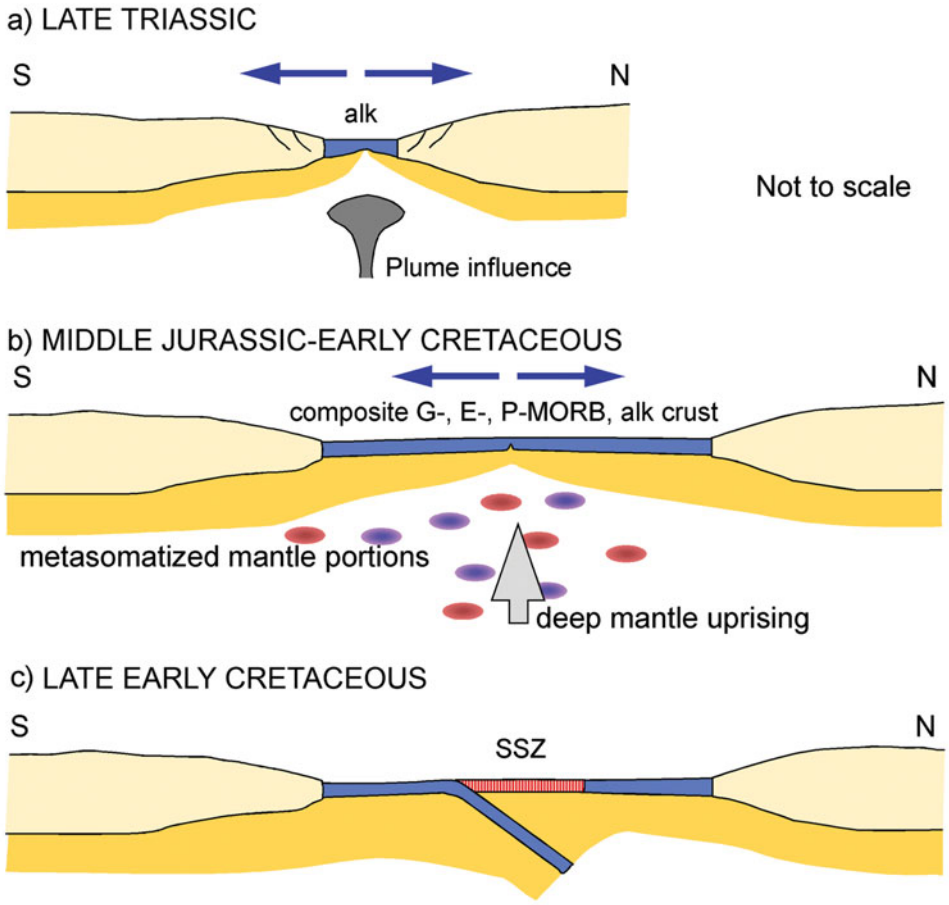

Figure 14. (Colour online) Two-dimensional cartoon showing the geodynamic evolution of the Izmir–Ankara Neotethys branch from Late Triassic to late Early Cretaceous times (modified from Göncüoglu, 2010). Abbreviations: MORB – mid-ocean ridge basalts; G- – garnet-influenced MORB; E- – enriched-MORB; P- – plume-type MORB; alk – alkaline basalts; SSZ – supra-subduction zone.

ridge setting by tapping different portions of a deep, highly heterogeneous mantle (Fig. 14b). Mantle heterogeneities consisted of portions variably enriched by OIB-type components, which were inherited from the Triassic mantle plume activity associated with the opening of this Neotethys oceanic branch (Fig. 14a). Our findings show that P-MORBs have a Middle Jurassic age, G-MORBs have a Late Jurassic age, E-MORBs were erupted during Early Cretaceous time and alkaline basalts were erupted from Late Jurassic to Early Cretaceous times. Partial melting of different portions of a heterogeneous sub-oceanic mantle (Figs 13, 14b) can explain the formation of different and genetically unrelated magmatic rocks in the same time span.

The intra-oceanic subduction likely started from late Early Cretaceous time on the northern side of the Neotethys branch, leading to the production of supra-subduction zone (SSZ)-type rocks during late Early Cretaceous time (Fig. 14c). Previous data on the earliest ages related to supra-subduction type volcanism and the formation of a metamorphic sole indicate an early Late Cretaceous age (e.g. T. Üner, unpub. Ph.D. thesis, Hacettepe Univ., 2010); therefore, the intra-oceanic decoupling within the ocean was considered as pre-Late Cretaceous in age. This age could not be verified in this study, since in contrast to the western part of the IAESB, none of the basalt samples collected from the eastern part yielded supra-subduction characteristics. The different rock types formed in the ocean were then incorporated into the accretionary prism during the Late Cretaceous closure.

7. Conclusion

This study is focused on slide blocks including oceanic lavas associated with pelagic sediments within the eastern part of the Ankara Mélange. A detailed petrological characterization of the volcanic rocks and a detailed biochronological investigation of the associated radiolarites was carried out. The main conclusions can be summarized as follows.

(1) The radiolarian cherts associated with volcanic rocks show the following ages: late Valanginian to late Hauterivian (Section 1, OIB); early–middle Bajocian to late Bathonian–early Callovian (Section 2, P-MORB); middle–late Oxfordian to late Kimmeridgian–early Tithonian (Section 3, OIB); middle late Barremian–early early Aptian (Section 4, E-MORB); middle late Oxfordian to late Kimmeridgian–early Tithonian and early–early late Tithonian (Section 5, G-MORB); Valanginian to

middle Aptian–early Albian (Section 7, E-MORB); late Valanginian–early Barremian (Section 8, G-MORB).

(2) Volcanic rocks are largely represented by basalts and minor ferrobasalts and trachytes. They show different geochemical affinities and overlapping ages including: (a) Late Jurassic – Early Cretaceous G-MORB; (b) Early Cretaceous E-MORB; (c) Middle Jurassic P-MORB; (d) Late Jurassic – Early Cretaceous alkaline basalts. All rock types show a clear garnet signature, as testified to by their high MREE/HREE ratios.

(3) REE modelling shows that their garnet signature is related to polybaric partial melting starting in the garnet peridotite stability field and continuing to larger degrees in the spinel-facies mantle. However, the different geochemical affinities displayed by the studied rocks are related to different mantle source compositions. G-MORBs were generated from 2.5 % melting in the garnet-facies and 10 % melting in the spinel-facies of a DMM source. E-MORB composition is compatible with mixing of melts derived from a very low degree (∼1 %) of partial melting of a DMM source in the garnet-facies with melts derived from a much larger degree (∼10 %) of partial melting in the spinel-facies mantle. Alternatively, these rocks may have derived from ∼8 % partial melting of a theoretical slightly enriched source in the spinel-facies. P-MORBs and alkaline basalts have REE compositions that can be accounted for by mixing of different proportions of melts generated in the garnet- and spinel-facies from an enriched mantle source metasomatized by OIB-type (plume-type) components.

(4) The coexistence of chemically different rock types from Middle Jurassic to Early Cretaceous times suggests that they were formed in a mid-ocean ridge setting from partial melting of a highly heterogeneous mantle characterized by the extensive occurrence of OIB-metasomatized portions, which were likely inherited from a Triassic mantle plume activity associated with the continental rift and opening of the Neotethys branch.

Acknowledgements. The Italian Ministry of Education, University and Research (MIUR) is acknowledged for the financial support (Prin 2010–2011). This research has also been funded by the Ferrara University (FIR-2016 Project). Many thanks go to Mirella Bonora (Ferrara University) for her support with analytical techniques. Radiolarian micrographs were taken with a Philips XL20 of the Ivalsa Institute (CNR) by Simona Lazzeri and with a Zeiss EVO MA15 of the MEMA (University of Florence) by Maurizio Ulivi. Special thanks go to Špela Goričan and anonymous reviewer for their constructive reviews of this paper.

Supplementary material

To view supplementary material for this article, please visit https://doi.org/10.1017/S0016756817000401.

References

Akal, C., Candan, O., Koralay, E., Oberhänsli, R., Chen, F. & Prelevic, D. 2012. Early Triassic potassic volcanism in the Afyon Zone of the Anatolides/Turkey: implications for the rifting of the Neo-Tethys. *International Journal of Earth Sciences* **101**, 177–94.

Aita, Y. & Okada, H. 1986. Radiolarians and calcareous nannofossils from the Uppermost Jurassic–Lower Cretaceous strata of Japan and Tethyan Regions. *Micropaleontology* **32**, 97–128.

Akbayram, K., Okay, A. I. & Satir, M. 2012. Early Cretaceous closure of the Intra-Pontide Ocean in western Pontides (northwestern Turkey). *Journal of Geodynamics* **65**, 38–55.

Aliev, K. 1967. New radiolarian species of the Valanginian and Albian Stages of northeastern Azerbaidzhan. In *Cretaceous Deposits of the Eastern Caucasus and Adjacent Areas (Biostratigraphy and Paleogeography)*, pp. 23–30. Academy of Sciences USSR, Ministry of Oil Industry USSR, Institute of Geology and of the Processing of Fuel Minerals, Laboratory of the Biostratigraphy of Oil- and Gas-bearing Areas.

Allahyari, K., Saccani, E., Pourmoafi, M., Beccaluva, L. & Masoudi, F. 2010. Petrology of mantle peridotites and intrusive mafic rocks from the Kermanshah ophiolitic complex (Zagros belt, Iran): implications for the geodynamic evolution of the Neo-Tethyan oceanic branch between Arabia and Iran. *Ofioliti* **35**, 71–90.

Allègre, C. J. & Minster, J. F. 1978. Quantitative models of trace element behaviour in magmatic processes. *Earth and Planetary Science Letters* **38**, 1–25.

Altiner, D., Koçyiğit, A., Farinacci, A., Nicosia, U. & Conti, M. A. 1991. Jurassic–Lower Cretaceous stratigraphy and paleogeographic evolution of the southern part of north-western Anatolia (Turkey). *Geologica Romana* **27**, 13–80.

Bailey, E. B. & McCallien, W. J. 1953. Serpentinite lavas, the Ankara Mélange, and the Anatolian Thrust. *Transactions of the Royal Society of Edinburgh* **57**, 403–42.

Bak, M. 1996. Cretaceous Radiolaria from Niedzica Succession of the Pieniny Klippen Belt in Polish Carpathians. *Acta Palaeontologica Polonica* **41**, 91–110.

Bak, M. 1999. Cretaceous radiolarian zonation in the Polish part of the Pieniny Klippen Belt (Western Carpathians). *Geologica Carpathica* **50**, 21–31.

Bandini, A. N., Baumgartner, P. O., Flores, K., Dumitrica, P. & Jackett, S. J. 2011. Early Jurassic to early Late Cretaceous radiolarians from the Santa Rosa accretionary complex (northwestern Costa Rica). *Ofioliti* **31**, 1–35.

Baumgartner, P. O., Bartolini, A. C., Carter, E. S., Conti, M., Cortese, G., Danelian, T., De Wever, P., Dumitrica, P., Dumitrica-Jud, R., Goričan, Š., Guex, J., Hull, D. M., Kito, N., Marcucci, M., Matsuoka, A., Murchey, B., O'Dogherty, L., Savary, J., Vishnevskaya, V., Widz, D. & Yao, A. 1995*a*. Middle Jurassic to Early Cretaceous radiolarian biochronology of Tethys based on Unitary Associations. In *Middle Jurassic to Lower Cretaceous Radiolaria of Tethys: Occurrences, Systematics, Biochronology* (eds P. O. Baumgartner, L. O'Dogherty, Š. Goričan, E. Urquhart, A. Pillevuit & P. De Wever), pp. 1013–48. Mémoires de Géologie, Lausanne, no. 23.

Baumgartner, P. O., Bjørklund, K. R., Caulet, J. P., De Wever, P., Kellogg, D., Labracherie, M., Nakaseko, K., Nishimura, A., Schaaf, A., Schimdt-Effing, R. & Yao, A. 1981. Eurorad II, 1980. Second European

meeting of radiolarian paleontologists: current research on Cenozoic and Mesozoic radiolarians. *Eclogae Geologicae Helvetiae* **74**, 1027–61.

Baumgartner, P. O., O'Dogherty, L., Goričan, Š., Dumitrica-Jud, R., Dumitrica, P., Pillevuit, A., Urquhart, E., Matsuoka, A., Danelian, T., Bartolini, A. C., Carter, E. S., De Wever, P., Kito, N., Marcucci, M. & Steiger, T. A. 1995*b*. Radiolarian catalogue and systematics of Middle Jurassic to Early Cretaceous Tethyan genera and species. In *Middle Jurassic to Lower Cretaceous Radiolaria of Tethys: Occurrences, Systematics, Biochronology* (eds P. O. Baumgartner, L. O'Dogherty, Š. Goričan, E. Urquhart, A. Pillevuit & P. De Wever), pp. 37–685. Mémoires de Géologie, Lausanne, no. 23.

Beker, J. A., Menzies, M. A., Thirlwall, M. F. & Macpherson, C. G. 1997. Petrogenesis of Quaternary intraplate volcanism, Sana'a, Yemen: implications for plume-lithosphere interaction and polybaric melt hybridization. *Journal of Petrology* **38**, 1359–90.

Berber, F., Göncüoglu, M. C. & Sayit, K. 2014. Geochemistry and tectonic significance of the Kösedag metavolcanic rocks from the Sakarya Zone, Northern Turkey. Bulletin. In *Proceedings of the 20th CBGA Congress 24-26 Sept 2014, Tirana* (eds A. Begiraj, C. Ionescu, G. Christofides, A. Uta, E. Beqiraj Goga & S. Marku). *Shkencave Gjeologjike Special Issue* **2**, 161–3.

Boccaletti, M., Bortolotti, V. & Sagri, M. 1966. Ricerche sulle ofioliti delle catene alpine: I. Osservazioni sull'Ankara Mélange nella zona di Ankara. *Bollettino della Società Geologica Italiana* **85**, 485–508.

Bortolotti, V. & Principi, G. 2005. Tethyan ophiolites and Pangea break-up. *The Island Arc* **14**, 442–70.

Bortolotti, V., Chiari, M., Göncüoglu, M. C., Marcucci, M., Principi, G., Tekin, U. K., Saccani, E. & Tassinari, R. 2013*a*. Age and geochemistry of basalt-chert associations in the ophiolitic complexes of the Izmir-Ankara Mélange East of Ankara, Turkey: preliminary data. *Ofioliti* **38**, 157–73.

Bortolotti, V., Chiari, M., Marroni, M., Pandolfi, L., Principi, G. & Saccani, E. 2013*b*. Geodynamic evolution of the ophiolites from Albania and Greece (Dinaric-Hellenic belt): one, two or more oceanic basins? *International Journal of Earth Sciences* **102**, 783–811.

Bortolotti, V. & Sagri, M. 1968. Ricerche sulle ofioliti delle catene alpine. 4 – Osservazioni sull'età e la giacitura delle ofioliti tra Smirne ed Erzurum (Turchia). *Bollettino della Società Geologica Italiana* **87**, 661–6.

Bragin, N. Yu. & Tekin, U. K. 1996. Age of radiolarian-chert blocks from the Senonian ophiolitic mélange (Ankara, Turkey). *The Island Arc* **5**, 114–22.

Brunelli, D., Seyler, M., Cipriani, A., Ottolini, L. & Bonatti, E. 2006. Discontinuous melt extraction and weak refertilization of mantle peridotites at the Vema Lithospheric Section (Mid-Atlantic Ridge). *Journal of Petrology* **47**, 745–71.

Catanzariti, R., Ellero, A., Göncüoglu, M. C., Marroni, M., Ottria, G. & Pandolfi, L. 2013. The Taraklı Flysch in the Boyali area (Sakarya Terrane, northern Turkey): implications for the tectonic history of the IntraPontide suture zone. *Comptes Rendus Geoscience*, **345**, 454–61.

Cater, J. M. L., Hanna, S. S., Ries, A. C. & Turner, P. 1991. Tertiary evolution of the Sivas Basin, central Turkey. *Tectonophysics* **195**, 29–46.

Cemen, I., Göncüoğlu, M. C., Erler, A., Kozlu, H. & Perinçek, D. 1993. Indentation tectonics and associated lateral extrusion in East, Southeast and Central Anatolia. *Geological Society of America, Programs and Abstract*s, A116–7.

Chiari, M., Bortolotti, V., Marcucci, M., Photiades, A., Principi, G. & Saccani, E. 2012. Radiolarian biostratigraphy and geochemistry of the Koziakas Massif ophiolites (Greece). *Bulletin de la Societé géologique de France* **183**, 289–309.

Chiari, M., Cobianchi, M. & Picotti, V. 2007. Integrated stratigraphy (radiolarians and calcareous nannofossils) of the Middle to Upper Jurassic Alpine radiolarites (Lombard Basin, Italy): constraints to their genetic interpretation. *Palaeogeography, Palaeoclimatology, Palaeoecology* **249**, 233–70.

Chiari, M., Marcucci, M. & Prela, M. 2004. Radiolarian assemblages from the Jurassic cherts of Albania: new data. *Ofioliti* **29**, 95–105.

Danelian, T. 2008. Diversity and biotic changes of Archaeodictyomitrid Radiolaria from the Aptian/Albian transition (OAE1b) of southern Albania. *Micropaleontology* **54**, 3–13.

Danelian, T., Tsikos, H., Gardin, S., Baudin, F., Bellier, J. P. & Emmanuel, L. 2004. Global and regional palaeoceanographic changes as recorded in the Mid-Cretaceous (Aptian–Albian) sequence of the Ionian zone (NW Greece). *Journal of the Geological Society, London* **161**, 703–9.

Dercourt, J., Zonenshain, L. P., Ricou, L. E., Kazminm, V. G., Le Pichon, X., Knipper, A. L., Grandjacquet, C., Sbortshikovm, I. M., Geyssant, J., Lepvrier, C., Pechersky, D. H., Boulin, J., Sibuet, J. C., Savostin, L. A., Sorokhtin, O., Westphal, M., Bazhenov, M. L., Lauer, J. P. & Biju-Duval, M. B. 1986. Geological evolution of the Tethys belt from the Atlantic to the Pamirs since the Lias. In *Evolution of the Tethys*(eds J. Aubouin, X. Le Pichon & A. S. Monin). *Tectonophysics* **123**, 241–315.

De Wever, P. 1982. Radiolaires du Trias et du Lias de la Téthys (systématique, stratigraphie). *Societé Géologique du Nord* **7**, 1–600.

Dilek, Y., Thy, P., Hacker, B. & Grundvig, S. 1999. Structure and petrology of Tauride ophiolites and mafic dike intrusions (Turkey): implications for the Neo-Tethyan Ocean. *Geological Society of America Bulletin* **111**, 1192–216.

Dumitrica, P. 1970. Cryptocephalic and cryptothoracic Nassellaria in some Mesozoic deposits of Romania. *Revue Roumaine de Géologie, Géophysique et Géographie (série Géologie)* **14**, 45–124.

Dumitrica, P. & Dumitrica-Jud, R. 1995. *Aurisaturnalis carinatus* (Foreman), an example of phyletic gradualism among Saturnalid-type radiolarians. *Revue de Micropaléontologie* **38**, 195–216.

Dumitrica, P., Immenhauser, A. & Dumitrica-Jud, R. 1997. Mesozoic radiolarian biostratigraphy from Masirah Ophiolite, Sultanate of Oman Part I: Middle Triassic, uppermost Jurassic and Lower Cretaceous Spumellarians and multisegmented Nassellarians. *Bulletin of the National Museum of Natural Sciences, Taiwan* **9**, 1–106.

Dumitrica, P. & Zügel, P. 2008. Early Tithonian Saturnalidae (Radiolaria) from the Solnhofen area (Southern Franconian Alb, southern Germany). *Paläontologische Zeitschrift* **82**, 55–84.

Ellero, A., Ottria, G., Marroni, M., Pandolfi, L. & Göncüoğlu, M. C. 2015*a*. Analysis of the North

Anatolian Shear Zone in Central Pontides (northern Turkey): insight for geometries and kinematics of deformation structures in a transpressional zone. *Journal of Structural Geology* **72**, 124–41.

Ellero, A., Ottria, G., Sayit, K., Catanzariti, R., Frassi, C., Göncüoğlu, M. C., Marroni, M. & Pandolfi, L. 2015*b*. Geological and geochemical evidence for a Late Cretaceous continental arc in the central Pontides, northern Turkey. *Ofioliti* **40**, 73–90.

Elmas, A. & Yiğitbaş, E. 2001. Ophiolite emplacement by strike-slip tectonics between the Pontide Zone and the Sakarya Zone in northwestern Anatolia, Turkey. *International Journal of Earth Sciences* **90**, 257–69.

Elmas, A. & Yiğitbaş, E. 2005. Comment on "Tectonic evolution of the Intra-Pontide suture zone in the Armutlu Peninsula, NW Turkey" by Robertson & Ustaömer. *Tectonophysics* **405**, 213–21.

Erdogan, B., Akay, C & Ugur, M. S. 1996. Geology of the Yozgat region and evolution of the collisional Çankırı basin. *International Geological Revue* **38**, 788–806.

Filippov, A. N. & Kemkin, I. V. 2005. First finds of Middle Jurassic and Early Cretaceous (Valanginian) radiolarian assemblages in the Western Sikhote-Alin: their paleogeographic and tectonic significance. *Doklady Earth Sciences* **405**, 1141–4.

Floyd, P. A., Göncüoglu, M. C., Winchester, J. A. & Yaliniz, M. K. 2000. Geochemical character and tectonic environment of Neotethyan ophiolitic fragments and metabasites in the Central Anatolian Crystalline Complex, Turkey. In *Tectonics and Magmatism in Turkey and the Surrounding Area* (eds E. Bozkurt, J. Winchester & J. A. Piper.), pp. 183–202. Geological Society of London, Special Publication no. 173.

Gökten, E. & Floyd, P. A. 2007. Stratigraphy and geochemistry of pillow basalts within the ophiolitic mélange of the Izmir-Ankara-Erzincan suture zone: implications for the geotectonic character of the northern branch of Neotethys. *International Journal of Earth Sciences (Geologische Rundschau)* **96**, 725–41.

Göncüoglu, M. C. 1992. Structural and stratigraphical framework of the Central Anatolian Tertiary basins. In *Introduction to the Early Paleogene of the Haymana-Polatlı Basin* (eds E. Sirel & E. Yazgan), pp. 1–11. Field Trip Guidebook. Ankara: General Direction of Mineral Resources Exploration.

Göncüoglu, M. C. 2010. *Introduction to the Geology of Turkey: Geodynamic Evolution of the Pre-Alpine and Alpine Terranes*. General Directorate of Mineral Resources Exploration Monography Series 5, 66 pp.

Göncüoglu, M. C. 2011. Geology of the Kütahya-Bolkardağ Belt. *Mineral Resources Exploration Bulletin* **142**, 223–77.

Göncüoglu, M. C., Dirik, K. & Kozlu, H. 1997. General characteristics of pre-Alpine and Alpine Terranes in Turkey: explanatory notes to the terrane map of Turkey. *Annales Géologiques des Pays Helléniques* **37**, 515–36.

Göncüoglu, M. C., Gürsu, S., Tekin, U. K. & Köksal, S. 2008. New data on the evolution of the Neotethyan oceanic branches in Turkey: late Jurassic ridge spreading in the Intra-Pontide branch. *Ofioliti* **33**, 153–64.

Göncüoglu, M. C., Marroni, M., Pandolfi, L., Ellero, A., Ottria, G., Catanzariti, R., Tekin, U. K. & Sayit, K. 2014. The Arkot Dağ Mélange in Araç area, central Turkey: evidence of its origin within the geodynamic evolution of the Intra-Pontide suture zone. *Journal of Asian Earth Sciences* **85**, 117–39.

Göncüoglu, M. C., Marroni, M., Sayit, K., Tekin, U. K., Pandolfi, L. & Ellero, A. 2012. The Ayli Dağ ophiolite sequence (Central-Northern Turkey): a fragment of Middle Jurassic oceanic lithosphere within the Intra-Pontide Suture Zone. *Ofioliti* **37**, 77–92.

Göncüoglu, M. C., Sayit, K. & Tekin, U. K. 2010. Oceanization of the northern Neotethys: geochemical evidence from ophiolitic mélange basalts within the İzmir-Ankara suture belt, NW Turkey. *Lithos* **116**, 175–87.

Göncüoglu, M. C., Tekin, U. K., Sayit, K., Bedi, Y. & Uzunçimen, S. 2015. Opening, evolution and closure of the Neotethyan oceanic branches in Anatolia as inferred by radiolarian research. *Radiolaria* **35**, 88–90.

Göncüoglu, M. C., Tekin, U. K. & Turhan, N. 2001. Geological meaning of the Late Carnian basalts blocks with radiolarites within the Late Cretaceous Central Sakarya ophiolitic complex (NW Anatolia). *Jeo 2000 Proceedings CD-54-6*: 6.

Göncüoglu, M. C., Turhan, N., Sentürk, K., Özcan, A. & Uysal, S. 2000. A geotraverse across NW Turkey: tectonic units of the Central Sakarya region and their tectonic evolution. In *Tectonics and Magmatism in Turkey and the Surrounding Area* (eds E. Bozkurt, J Winchester & J.A. Piper), pp. 139–61. Geological Society of London, Special Publication no. 173.

Göncüoglu, M. C., Turhan, N. & Tekin, U. K. 2003. Evidence for the Triassic rifting and opening of the Neotethyan Izmir-Ankara Ocean, northern edge of the Tauride-Anatolide platform, Turkey. *Bollettino della Società Geologica Italiana, Special Volume* **2**, 203–12.

Göncüoglu, M. C., Yaliniz, K. & Tekin, U. K. 2006. Geochemistry, tectono-magmatic discrimination and radiolarian ages of basic extrusives within the Izmir-Ankara Suture Belt (NW Turkey): time constraints for the Neotethyan evolution. *Ofioliti* **31**, 25–38.

Goričan, Š. 1994. Jurassic and Cretaceous radiolarian biostratigraphy and sedimentary evolution of the Budva Zone (Dinarides, Montenegro). *Mémoires de Géologie, Lausanne* **18**, 1–120.

Goričan, Š., Pavšič, J. & Rožič, B. 2012. Bajocian to Tithonian age of radiolarian cherts in the Tolmin basin (NW Slovenia). *Bulletin de la Société géologique de France* **183**, 369–82.

Gülyüz, E., Kaymakci, N., Meijers, M. J. M., van Hinsbergen, D. J. J., Lefebvre, C., Vissers, R. L. M., Bart, W. H., Hendriks, B. W. H. & Peynircioglu, A. A. 2013. Late Eocene evolution of the Çiçekdağı Basin (central Turkey): syn-sedimentary compression during microcontinent-continent collision in central Anatolia. *Tectonophysics*. **602**, 286–99.

Hanan, B. B., Blichert-Toft, J., Kingsley, R. & Schilling, J. G. 2000. Depleted Iceland mantle plume geochemical signature: artifact of multicomponent mixing? *Geochemistry, Geophysics, Geosystems* **1**, 1–19.

Hubert-Ferrari, A., Armijo, R., King, G., Meyer, B. & Barka, A. 2002. Morphology, displacement, and slip rates along the North Anatolian Fault, Turkey. *Journal of Geophysical Research* **107**, ETG 9-1–ETG 9-33.

Irving, A. J. & Frey, F. A. 1984. Trace element abundances in megacrysts and their host basalts: constraints on partition coefficients and megacryst genesis. *Geochimica et Cosmochimica Acta* **48**, 1201–21.

Jackson, M. L. 1958. *Soil Chemical Analysis*. Englewood Cliffs, NJ: Prentice-Hall, 498 pp.

Kawabata, K. 1988. New species of Latest Jurassic and Earliest Cretaceous radiolarians from the Sorachi group in Hokkaido, Japan. *Bulletin of the Osaka Museum of Natural History* **43**, 1–13.

Kaymakci, N., Duermeijer, C. E., Langereis, C., White, S. H. & van Dijk, P. M. 2003. Palaeomagnetic

evolution of the Çankırı Basin (Central Anatolia, Turkey: implication for oroclinal bending due to indentation. *Geological Magazine* **140**, 343–55.

Kocyigit, A., Türkmenoglu, A., Beyhan, A., Kaymakçi, N. & Akyol, E. 1995. Post-collisional tectonics of Eskisehir-Ankara-Çankırı segment of Izmir-Ankara-Erzincan Suture Zone. *Turkish Association of Petroleum Geologists Bulletin* **6**, 69–87.

Köksal, S. & Göncüoglu, C. M. 2008. Sr and Nd isotopic characteristics of some S-, I- and A-type granitoids from Central Anatolia. *Turkish Journal of Earth Sciences* **17**, 111–27.

Kozur, H. 1985. The radiolarian genus *Eoxitus* n. gen from the *Unuma echinatus* zone (Bajocian) of Northern Hungary. *Proceed Koninklijke Nederoands Academie Van Wetenscappen*, **88**, 211–20.

Lachance, G. R. & Trail, R. J. 1966. Practical solution to the matrix problem in X-ray analysis. *Canadian Spectroscopy* **11**, 43–48.

Liu, C.-Z., Snow, J. E., Hellebrand, E., Brügmann, G. E., von der Handt, A. B. & Hofmann, A. W. 2008. Ancient, highly heterogeneous mantle beneath Gakkel ridge. Arctic Ocean. *Nature* **452**, 311–6.

McKenzie, D. & O'Nions, R. K. 1991. Partial melt distributions from inversion of rare Earth element concentrations. *Journal of Petrology* **32**, 1021–91.

Moix, P., Beccaletto, L., Kozur, H. W., Hochard, C., Rosselet, F. & Stampfli, G. M. 2008. A new classification of the Turkish terranes and sutures and its implication for the paleotectonic history of the region. *Tectonophysics* **451**, 7–39.

Moix, P. & Goričan, Š. 2013. Jurassic and Cretaceous radiolarian assemblages from the Bornova mélange in northern Karaburun Peninsula (western Turkey) and its connection to the İzmir-Ankara mélanges. *Geodinamica Acta* **26**, 56–67.

Montanini, A., Tribuzio, R. & Vernia, L. 2008. Petrogenesis of basalts and gabbros from an ancient continent-ocean transition (External Liguride ophiolites, Northern Italy). *Lithos* **101**, 453–79.

O'Dogherty, L. 1994. Biochronology and paleontology of Mid-Cretaceous radiolarians from Northern Apennines (Italy) and Betic Cordillera (Spain). *Mémoires de Géologie, Lausanne* **21**, 1–415.

O'Dogherty, L., Carter, E. S., Dumitrica, P., Goričan, Š., De Wever, P., Bandini, A. N., Baumgartner, P. O. & Matsuoka, A. 2009. Catalogue of Mesozoic radiolarian genera. Part 2: Jurassic–Cretaceous. *Geodiversitas* **31**, 271–356.

Okay, A. I. & Göncüoglu, M. C. 2004. The Karakaya Complex: a review of data and concepts. *Turkish Journal of Earth Sciences* **13**, 75–95.

Okay, A. I. & Tüysüz, O. 1999. Tethyan sutures of northern Turkey. In *The Mediterranean Basin: Tertiary Extension within the Alpine Orogen* (eds B. Durand, L. Jolivet, F. Horváth & M. Séranne), pp. 475–515. Geological Society of London, Special Publication no. 156.

Parlak, O., Çolakoğlu, A., Dönmez, C., Sayak, H., Yildirim, N., Türkel, A. & Odabaşi, İ. 2013. Geochemistry and tectonic significance of ophiolites along the İzmir-Ankara-Erzincan Suture Zone in northeastern Anatolia. In *Geological Development of Anatolia and the Easternmost Mediterranean* (eds A. H. F. Robertson, O. Parlak & U. Unlugenc), pp. 75–105. Geological Society of London, Special Publication no. 372.

Pearce, J. A. 1982. Trace element characteristics of lavas from destructive plate boundaries. In *Andesites* (ed. R. S. Thorpe), pp. 525–48. New York: John Wiley & Sons.

Pearce, J. A. & Norry, M. J. 1979. Petrogenetic implications of Ti, Zr, Y, and Nb variations in volcanic rocks. *Contributions to Mineralogy and Petrology* **6**, 33–47.

Pessagno, E. A. & Newport, L. A. 1972. A technique for extracting Radiolaria from radiolarian chert. *Micropaleontology* **18**, 231–4.

Robertson, A. H. F., Dixon, J. E., Brown, S., Collins, A., Morris, A., Pickett, E. A., Sharp, I. & Ustaömer, T. 1996. Alternative tectonic models for the Late Palaeozoic–Early Tertiary development of Tethys in the Eastern Mediterranean region. In *Palaeomagnetism and Tectonics of the Mediterranean Region* (eds A. Morris & D. H. Tarling), pp. 239–63. Geological Society of London, Special Publication no. 105.

Robertson, A., Parlak, O., Ustaömer, T., Tasli, K., İnan, N., Dumitrica, P. & Karaoğlan, F. 2013. Subduction, ophiolite genesis and collision history of Tethys adjacent to the Eurasian continental margin: new evidence from the Eastern Pontides, Turkey. *Geodinamica Acta* **26**, 230–93.

Robertson, A. H. F. & Ustaömer, T. 2004. Tectonic evolution of the Intra-Pontide suture zone in the Armutlu Peninsula, NW Turkey. *Tectonophysics* **381**, 175–209.

Robin, C., Goričan, Š., Guillocheau, F., Razin, P., Dromart, G. & Mosaffa, H. 2010. Mesozoic deep-water carbonate deposits from the southern Tethyan passive margin in Iran (Pichakun nappes, Neyriz area): biostratigraphy, facies sedimentology and sequence stratigraphy. In *Tectonic and Stratigraphic Evolution of Zagros and Makran during the Mesozoic–Cenozoic* (eds P. Leturmy & C. Robin), pp. 179–210. Geological Society of London, Special Publication no. 330.

Rojay, B. 2013. Tectonic evolution of the Cretaceous Ankara Ophiolitic Mélange during the Late Cretaceous to pre-Miocene interval in Central Anatolia, Turkey. *Journal of Geodynamics* **65**, 66–81.

Rojay, B., Yaliniz, M. K. & Altiner, D. 2001. Tectonic implications of some Cretaceous pillow basalts from the North Anatolian Ophiolitic Mélange (Central Anatolia-Turkey) to the evolution of Neotethys. *Turkish Journal of Earth Sciences* **10**, 93–102.

Saccani, E. 2015. A new method of discriminating different types of post-Archean ophiolitic basalts and their tectonic significance using Th-Nb and Ce-Dy-Yb systematics. *Geoscience Frontiers* **6**, 481–501.

Saccani, E., Allahyari, K., Beccaluva, L. & Bianchini, G. 2013*a*. Geochemistry and petrology of the Kermanshah ophiolites (Iran): implication for the interaction between passive rifting, oceanic accretion, and plume-components in the Southern Neo-Tethys Ocean. *Gondwana Research* **24**, 392–411.

Saccani, E., Azimzadeh, Z., Dilek, Y. & Jahangiri, A. 2013*b*. Geochronology and petrology of the Early Carboniferous Misho Mafic Complex (NW Iran), and implications for the melt evolution of Paleo-Tethyan rifting in Western Cimmeria. *Lithos* **162-163**, 264–78.

Saccani, E., Beccaluva, L., Photiades, A. & Zeda, O. 2011. Petrogenesis and tectono-magmatic significance of basalts and mantle peridotites from the Albanian-Greek ophiolites and sub-ophiolitic mélanges. New constraints for the Triassic-Jurassic evolution of the Neo-Tethys in the Dinaride sector. *Lithos* **124**, 227–42.

Saccani, E., Delavari, M., Beccaluva, L. & Amini, S. A. 2010. Petrological and geochemical constraints on the origin of the Nehbandan ophiolitic complex (eastern

Iran): implication for the evolution of the Sistan Ocean. *Lithos* **117**, 209–28.

Saccani, E. & Photiades, A. 2005. Petrogenesis and tectono-magmatic significance of volcanic and subvolcanic rocks in the Albanide-Hellenide ophiolitic mélanges. *The Island Arc* **14**, 494–516.

Saccani, E., Photiades, A., Santato, A. & Zeda, O. 2008*a*. New evidence for supra-subduction zone ophiolites in the Vardar Zone from the Vermion Massif (northern Greece): implication for the tectono-magmatic evolution of the Vardar oceanic basin. *Ofioliti* **33**, 65–85.

Saccani, E. & Principi, G. 2016. Petrological and tectono-magmatic significance of ophiolitic basalts from the Elba Island within the Alpine Corsica-Northern Apennine system. *Mineralogy and Petrology* **110**, 713–30.

Saccani, E., Principi, G., Garfagnoli, F. & Menna, F. 2008*b*. Corsica ophiolites: geochemistry and petrogenesis of basaltic and metabasaltic rocks. *Ofioliti* **33**, 187–207.

Sayit, K., Tekin, U. K. & Göncüoglu, M. C. 2011. Early-Middle Carnian radiolarian cherts within the Eymir Unit, Central Turkey: constraints for the age of the Palaeotethyan Karakaya Complex. *Journal of Asian Earth Sciences* **42**, 398–407.

Schmid, S. M., Bernoulli, D., Fügenschuh, B., Matenco, L., Schefer, S., Schuster, R., Tischler, M. & Ustaszewski, K. 2008. The Alpine-Carphatian-Dinaridic orogenic system: correlation and evolution of tectonic units. *Swiss Journal of Geosciences* **101**, 139–83.

Sengör, A. M. C. & Yilmaz, Y. 1981. Tethyan evolution of Turkey: a plate tectonic approach. *Tectonophysics* **75**, 181–241.

Smuc, A. & Goričan, Š. 2005. Jurassic sedimentary evolution of a carbonate platform into a deep-water basin, Mt. Mangart (Slovenian–Italian Border). *Rivista Italiana di Paleontologia e Stratigrafia* **111**, 45–70.

Soycan, H., Erdoğan, K. & Konak, N. 2015. Aalenian–Early Bathonian (Middle Jurassic) radiolarian assemblages in the Tavas nappe within Lycian nappes in the western Taurides (SW Turkey): the first dating of carbonate platform drowning. *Journal of Asian Earth Sciences*, **104**, 3–21.

Stampfli, G. M. & Borel, G. D. 2002. A plate tectonic model for the Palaeozoic and Mesozoic constrained by dynamic plate boundaries and restored synthetic oceanic isochrones. *Earth and Planetary Science Letters* **169**, 17–33.

Sun, S. S. & McDonough, W. F. 1989. Chemical and isotopic-systematics of oceanic basalts: implications for mantle composition and processes. In *Magmatism in the Ocean Basins* (eds A. D. Saunders & M. J. Norry), pp. 313–45. Geological Society of London, Special Publication no. 42.

Tekin, U. K. 1999. Biostratigraphy and systematics of Late Middle to Late Triassic radiolarians from the Taurus Mountains and Ankara region, Turkey. *Geologische und Paläontologische Mitteilungen Innsbruck, Sonderband* **5**, 1–296.

Tekin, U. K. & Göncüoglu, M. C. 2007. Discovery of the oldest (Upper Ladinian to Middle Carnian) radiolarian assemblages from the Bornova Flysch Zone in western Turkey: implications for the evolution of the Neotethyan Izmir-Ankara Ocean. *Ofioliti* **32**, 131–50.

Tekin, U. K. & Göncüoglu, M. C. 2009. Late Middle Jurassic (late Bathonian–early Callovian) radiolarian cherts from the Neotethyan Bornova Flysch Zone, Spil Mountains, Western Turkey. *Stratigraphical and Geological Correlation* **17**, 298–308.

Tekin, U. K., Göncüoğlu, M. C., Pandolfi, L. & Marroni, M. 2012. Middle–Late Triassic radiolarian cherts from the Arkotdağ mélange in northern Turkey: implications for the life span of the northern Neotethyan branch *Geodinamica Acta* **25**, 305–19.

Tekin, U. K., Göncüoglu, M. C. & Turhan, N. 2002. First evidence of Late Carnian radiolarian fauna from the Izmir-Ankara Suture Complex, Central Sakarya, Turkey: implications for the opening age of the Izmir-Ankara branch of Neotethys. *Geobios* **35**, 127–35.

Tekin, U. K., Göncüoglu, M. C & Uzuncimen, S. 2012. Radiolarian assemblages of Middle and Late Jurassic to early Late Cretaceous (Cenomanian) ages from an olistolith record pelagic deposition within the Bornova Flysch Zone in western Turkey. *Bulletin de la Societé géologique de France* **183**, 307–18.

Thirlwall, M., Upton, B. G. J. & Jenkins, C. 1994. Interaction between continental lithosphere and the Iceland plume-Sr-Nd-Pb isotope geochemistry of Tertiary basalts, NE Greenland. *Journal of Petrology* **35**, 839–79.

Topuz, G., Çelik, Ö. F., Şengör, A. M. C., Altintaş, İ. E., Zack, T., Rolland, Y. & Barth, M. 2013*a*. Jurassic ophiolite formation and emplacement as backstop to a subduction-accretion complex in northeast Turkey, the Refahiye ophiolite, and relation to the Balkans ophiolites. *American Journal of Science* **313**, 1054–87.

Topuz, G., Göçmengil, G., Rolland, Y., Çelik, Ö. F., Zack, T. & Schmitt, A. K. 2013*b*. Jurassic accretionary complex and ophiolite from northeast Turkey: no evidence for the Cimmerian continental ribbon. *Geology* **45**, 255–8.

Warren, J. M. 2016. Global variations in abyssal peridotite compositions. *Lithos* **248-251**, 193–219.

Warren, J. M., Shimizu, N., Sakaguchi, C., Dick, H. J. B. & Nakamura, E. 2009. An assessment of upper mantle heterogeneity based on abyssal peridotite isotopic compositions. *Journal of Geophysical Research* **114**, B12203, doi: 10.1029/2008JB006186.

Wood, D. A. 1980. The application of a Th-Hf-Ta diagram to problems of tectonomagmatic classification and to establishing the nature of crustal contamination of basaltic lavas of the British Tertiary volcanic province. *Earth and Planetary Science Letters* **50**, 11–30.

Workman, R. K. & Hart, S. R. 2005. Major and trace element composition of the DMM. *Earth and Planetary Science Letters* **2**, 53–72.

Yaliniz, M. K., Floyd, P. A. & Göncüoglu, M. C. 1996. Supra-subduction zone ophiolites of Central Anatolia: geochemical evidence from the Sarıkaraman Ophiolite, Aksaray. *Turkish Mineralogical Magazine* **60**, 697–710.

Yaliniz, K., Göncüoglu, M. C. & Floyd, P. A. 2000. Geochemistry of volcanic rocks from the Çicekdağ Ophiolite, Central Anatolia, Turkey, and their inferred tectonic setting within the northern branch of the Neotethyan ocean. In *Tectonics and Magmatism in Turkey and the Surrounding Area* (eds E. Bozkurt, J. Winchester & J. A. Piper), pp. 203–18. Geological Society of London, Special Publication no. 173.

Yaliniz, M. K., Göncüoglu, M. C. & Özkan-Altiner, S. 2000. Formation and emplacement ages of the SSZ-type Neotethyan ophiolites in Central Anatolia, Turkey: paleotectonic implications. *Geological Journal* **35**, 53–68.

Yilmaz, Y., Serdar, H. S., Genc, C., Yigitbas, E., Gurer, F., Elmas, A., Yildirim, M., Bozcu, M. & Gurpinar, O. 1997. The geology and evolution of the Tokat Massif, south central Pontides, Turkey. *International Geological Revue* **39**, 365–82.

Yolsal-Çevikbilen, S., Biryol, C. B., Beck, S., Zandt, G., Taymaz, T., Adiyaman, H. E. & Özacar, A. A. 2012. 3-D crustal structure along the North Anatolian Fault Zone in north-central Anatolia revealed by local earthquake tomography. *Geophysical Journal International* **188**, 819–49.